Design of an Experimental Loop for Post-LOCA Heat Transfer Regimes in a Gas-Cooled Fast Reactor
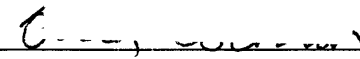
by

Peter A. Cochran

B.S. Nuclear Engineering
University of Illinois at Urbana-Champaign, 2002

Submitted to the Department of Nuclear Engineering in
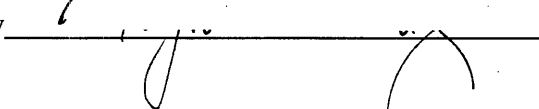partial fulfillment of the requirements for the Degree of

Master of Science in Nuclear Engineering
At the
Massachusetts Institute of Technology

February 2005

Author_____

<div align="right">

Department of Nuclear Engineering
January 17, 2004

</div>

Certified by_____

<div align="right">

Pavel Hejzlar
Principal Research Scientist
Thesis Supervisor

</div>

Certified by_____

<div align="right">

Mujid Kazimi
Nuclear Engineering Professor
Thesis Reader

</div>

Accepted by_____

<div align="right">

Jeff Coderre
Nuclear Engineering Professor
Chairman, Committee for Graduate Studies

</div>

1

Design of an Experimental Loop for Post-LOCA
Heat Transfer Regimes in a Gas-Cooled Fast Reactor

by

Peter A. Cochran

Abstract

The goal of this thesis is to design an experimental thermal-hydraulic loop capable of generating accurate, reliable data in various convection heat transfer regimes for use in the formulation of a comprehensive convection heat transfer correlation. The initial focus of the design is to ensure that the loop will be able to generate the convection flow regimes found in post Loss of Coolant Accident (LOCA) operation of a Gas-cooled Fast Reactor (GFR). As a result a scaling analysis of the proposed test facility was undertaken to demonstrate that the proposed loop would be able to operate in these aforementioned regimes. Having verified that the experimental loop could operate in the regimes of interest the next stage in the project was construction of the loop. Following construction of the loop and necessary instrumentation, an uncertainty analysis of the facility was conducted with the goal of determining the uncertainty associated with the calculation of heat transfer coefficients from the experimental data. The initial results were discouraging as the uncertainty calculated was large, ranging from ~10-60%. After performing a heat transfer coefficient uncertainty analysis, we observed that the bulk of the uncertainty was due to heat loss from the fluid to the environment. Therefore, guard heaters were implemented into the loop design, to match the inner surface temperature of the insulation to the wall temperature of the test section, which allows minimization of heat loss to about zero. This resulted in the considerable reduction in heat transfer coefficient uncertainty to ~8-15%.

Thesis Reader: Mujid Kazimi

Title: Professor of Nuclear Engineering

Acknowledgements

Table of Contents

List of Figures

List of Tables

1. INTRODUCTION

The next generation of nuclear reactors, commonly referred to as Generation IV reactors, is currently in the initial stages of design. One of the most promising Generation IV reactor concepts is the Gas-Cooled Fast Reactor (GFR) with a block-core configuration, first proposed at MIT [Hejzlar 2001]. Historically, one of the main concerns with gas-cooled reactors is the inherently poor heat transfer of gases. This is quite problematic in a Loss-of-Coolant-Accident (LOCA) as the reduced coolant flow must still be able to ensure adequate decay heat removal from the reactor. In the past gas-cooled reactor designs implemented electric blowers to increase coolant flow following a LOCA. [Gratton 1981] However the Generation IV reactor initiative has placed particular emphasis on passive safety systems. As a result convection loops, connecting the core to elevated heat exchangers and operating under natural circulation, were chosen as a possible means of passively cooling the core following a LOCA. In order to determine the heat transfer capabilities of such a system, an analysis was undertaken to determine the convection flow regimes of the naturally circulating coolant. [Williams et al. 2003] The results of the analysis are depicted in Figure 1-1.

8
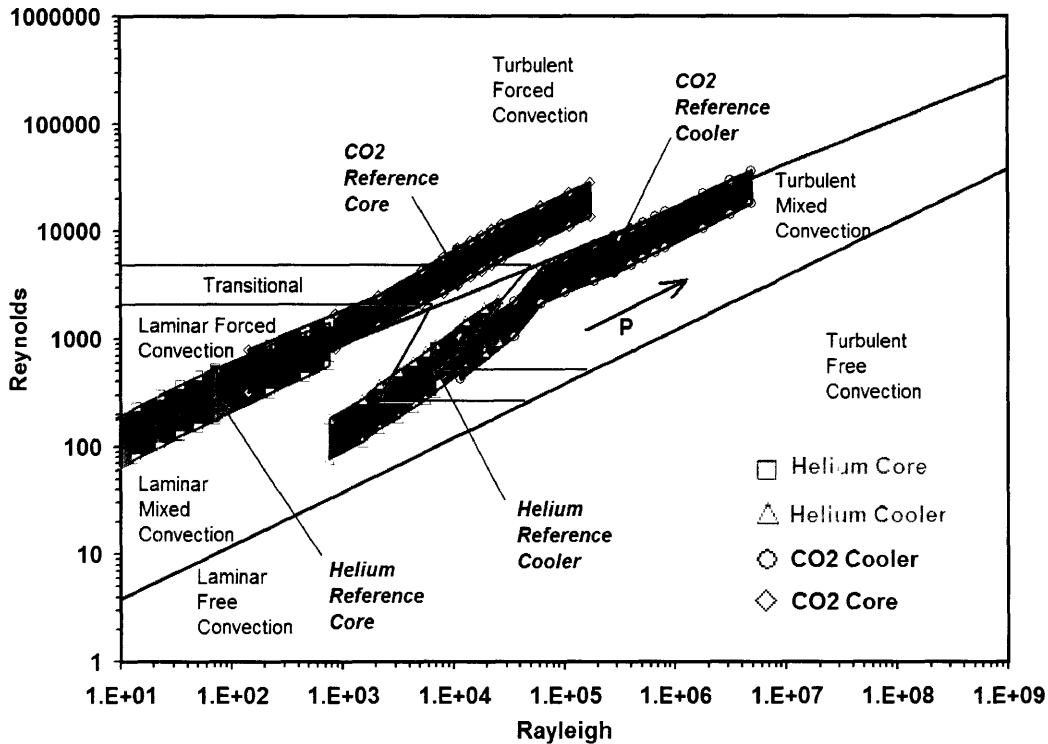
Figure 1-1 Convection flow regimes at various operating pressures for both
Helium and CO_2 (from Williams et al., 2003)

In addition to operating in the well-understood turbulent forced convection regime, the

convection loops also operate in lesser-known regimes, such as mixed convection and in the

transition regimes between forced and mixed convection and laminar and turbulent flow. One of

the reasons heat transfer in the aforementioned regimes is not well understood is, that in the past,

researchers have taken a piecemeal approach to developing heat transfer correlations for

convection flow regimes. This approach is understandable as there are nine possible convective

heat transfer regimes listed in Table 1-1.

9

Table 1-1 Possible flow and heat transfer regimes

Regime	Turbulent	Transition	Laminar
Forced	X	X	X
Mixed	X	X	X
Free	X	X	X

However this approach has created two significant problems. First there are significant gaps in both experimental and theoretical knowledge for mixed and transition convection regimes. Secondly the lack of a broad, unified approach to understanding convection flow regimes precludes any chance of formulating a comprehensive convection heat transfer correlation. These two problems provided the impetus for the heat transfer project to be begun in this thesis. The goal of the project is to fill in the experimental gaps in convection flow regimes and develop a comprehensive convection heat transfer correlation.

The specific goal of this thesis is to lay the groundwork for the experimental work to be undertaken by designing and constructing a thermal-hydraulic loop capable of operating in a variety of convection regimes. The basis for the design of the loop will be the natural circulation convection loops analyzed for the GFR, however modifications will be made to encompass as many of the flow regimes mentioned in Table 1-1 as possible.

References

1. Gratton C.P., "The Gas-Cooled Fast Reactor in 1981," Nuclear Energy, Vol. 20, No.4, pp. 287-295 (1981).

2. Hejzlar P., Driscoll M.J., and Todreas N.E., "The Long-Life Modular Gas Turbine Fast Reactor Concept," International Congress on Advanced Nuclear Power Plants, Hollywood, Florida, June 9-13, 2002.

3. Williams, W., Hejzlar, P., Driscoll, M. J., Lee, W-J. and Saha, P., (2003), "Analysis of a Convection Loop for GFR Post-LOCA Decay Heat Removal from a Block-Type Core," MIT-ANP-TR-095, March 2003.

2. BACKGROUND

2.1 Determining Convective Flow Regimes

Heat transfer in a convective system is accomplished by motion of the fluid. In free convection buoyancy forces due to the temperature difference between the fluid and its surroundings gives rise to a localized flow of the fluid. In forced convection an external force such as a pressure differential drives fluid flow. When both free and forced convection are present the system is said to be operating in a mixed convection regime. The combination of these three forms of convection along with laminar, transitional, and turbulent flows result in the nine possible heat transfer and flow regimes of Table 1-1. In order to determine the important parameters for determining the heat transfer regime a dimensional analysis of the governing equations of momentum and energy must be undertaken. Such an analysis was conducted for upward heated flow in a round tube at MIT. [Parlatan 1993] The momentum and energy equations were put in their non-dimensional forms through application of the following characteristic quantities and their resulting non-dimensional variables.

Characteristic Quantities

V characteristic velocity,

D characteristic length (tube inside diameter)

ρ_o fluid centerline density

T_w wall inside temperature

T_o fluid centerline temperature

Non-Dimensional Variables

$$u^* = \frac{u}{V}$$

$$r^* = \frac{r}{D}$$

$$z^* = \frac{z}{D}$$

$$\tilde{p}^* = \frac{\tilde{p}}{\rho_o V^2}$$

$$t^* = \frac{t}{(D/V)}$$

$$T^* = \frac{T - T_o}{T_w - T_o}$$

The resultant non-dimensional energy and momentum equations are as follows; [Parlatan 1993]

$$0 = \frac{Gr}{Re^2} T^* - \frac{\partial \tilde{p}^*}{\partial z^*} + \frac{1}{r^*} \frac{\partial}{\partial r^*} \left[\left[\frac{1}{Re} + \frac{\mu_t}{\rho VD} \right] r^* \frac{\partial u^*}{\partial r^*} \right] \tag{2-1}$$

$$Re \frac{\partial T^*}{\partial z^*} = \frac{1}{r^*} \frac{\partial}{\partial r^*} \left[\left[\frac{1}{Pr} + \frac{\alpha_t}{\nu} \right] r^* \frac{\partial T^*}{\partial r^*} \right] + \frac{\partial}{\partial z^*} \left[\left[\frac{1}{Pr} + \frac{\alpha_t}{\nu} \right] \frac{\partial T^*}{\partial z^*} \right] \tag{2-2}$$

The three important non-dimensional parameters from the above equations are:

Re = $\rho VD/\mu$ = VD/ν (Reynolds Number)

Pr = $\mu c_p/k$ = ν/α (Prandtl Number)

$Gr_{\Delta T}$ = Gr = $g\beta(T_w-T_o)D^3/\nu^2$ (Grashof Number)

The fact that two of these non-dimensional parameters, Gr and Re, are important for mixed convective flow comes as no surprise as the Gr number is indicative of the buoyant forces

13

involved in free convection while the Re number represents the pressure gradient forces that drive forced convection. The Pr number on the other hand is important for convection in general as it is a ratio of momentum diffusivity (convection) to thermal diffusivity (conduction). However as the Pr number has a constant value of approximately 0.7 for most gases its use in defining convective flow as either free, forced, or mixed is of limited value. It should also be noted at this point that most convection flow regimes are plotted on a Ra (Gr x Pr) vs. Re number graph. This is due to the fact that researchers believe that the Ra (Gr x Pr) number is better suited than the Gr number to determine growth of the thermal boundary layer and resulting heat transfer coefficients in free convection. [Bejan 1993]

Having determined the appropriate backdrop for plotting convection regimes, the next step is to determine the boundaries between forced, mixed, and free convection. Forced convection transitions to mixed convection as the result of the onset of buoyancy influenced convection. Aicher and Martin [1997] proposed the following criterion to serve as the boundary between forced and mixed convection:

$$Ra^{0.333}/(Re^{0.8} \, Pr^{0.4}) = 0.05 \qquad (2\text{-}3)$$

The previous equation can be further simplified if the Pr number is assumed to be a constant 0.7, as is the case for most gases.

$$Ra^{0.333}/Re^{0.8} = 0.04335 \qquad (2\text{-}4)$$

The transition between mixed and free convection occurs as buoyancy influenced convection becomes the dominant mechanism in heat transfer of the fluid. Burmeister [1993] proposed to use the ratio of Gr/Re^2 to demarcate between mixed and free convection. He reasoned that the ratio of buoyancy forces (Gr) to inertial forces (Re) should be greater than unity for free convection to be dominant.

$$Gr/Re^2 = 1 \qquad (2\text{-}5)$$

14

Multiplying both sides of equation 2-5 by the Pr number results in the following criterion for demarcation between mixed and free convection:

$$Ra/Re^2 = 0.7 \qquad (2\text{-}6)$$

Application of equations 2-4 and 2-6 to the Ra vs. Re plot results in the following convection flow regime map:
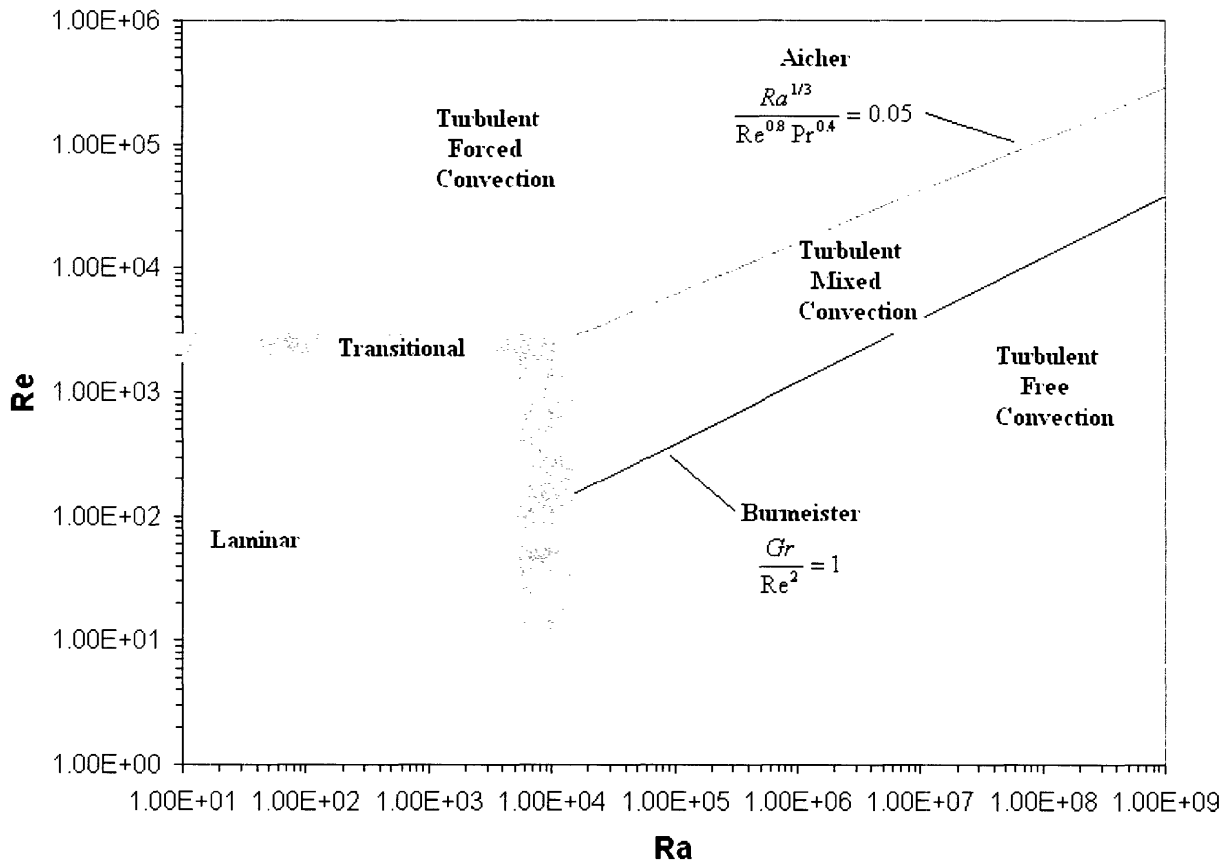
Figure 2-1 Tentative Forced-mixed-free convection boundaries for Pr = 0.7

It is important to note that proposed boundaries between forced and mixed convection and mixed and free convection are limited to turbulent flow. In the transition regime between laminar and turbulent flow no guidelines exist for distinguishing between the convective flows. And in the laminar regime it is not necessary to distinguish between free, mixed, and forced convection as the Nusselt number can be expressed as a combination of free and forced convection. [Churchill

15

1998]It is also important to emphasize that Figure 2-1 is a tentative flow regime map; the boundaries between the convective flows need to be verified experimentally. Failing in that, new boundaries between the flow regimes would need to be proposed.

In addition to simply relying on Ra and Re numbers to define convection flow regimes two other parameters; the Buoyancy parameter, Bo*, and the Acceleration parameter, K_v, will be used to help identify convection flow regimes. Jackson and co-workers [1989] introduced the Buoyancy parameter to determine the onset of buoyancy-influenced convection in turbulent flow. The Buoyancy parameter is given by the following expression:

$$Bo^* = Gr^* / (Re^{3.425} Pr^{0.8}) \qquad (2-7)$$

In the preceding equation Gr* is simply the Grashof number based on wall heat flux instead of the temperature difference between the wall and bulk fluid. Jackson [1998] proposed that the onset of buoyancy influenced convection for gas flow in round tubes would occur at Bo* = 5 x 10^{-7}.

The Acceleration parameter, K_v, is important as it accounts for the process of laminarization whereby turbulent flows exhibit the lower heat transfer characteristics of laminar flows. [Bankston 1970]

$$K_v = 4 (q_w^{''}/Gc_pT_b)/(V_bD/v) = 4q^+/Re \qquad (2-8)$$

We will mainly use the acceleration parameter to determine whether laminarization of the flow is contributing to the decrease in the heat transfer when the flow transitions between turbulent convection regimes.

In summation there are 4 important non-dimensional parameters in determining convection flow regimes; Ra(Gr), Re, Bo*, and K_v. These four parameters will provide the basis for design of the experimental thermal-hydraulic loop.

2.2 Existing Heat Transfer Correlations and Experimental Data

In order to formulate a comprehensive heat transfer correlation for convective flow regimes, a theoretical basis must be determined for developing the heat transfer correlation and experimental data covering the entire range of convective flows must be acquired to verify the validity of the correlation. It is instructive in developing a heat transfer correlation to first look at the various heat transfer correlations already in existence for convection flow regimes. Figure 2-1 is easily divided into three heat transfer regimes; laminar, transitional, and turbulent convection.

As mentioned in the previous section Churchill [1998] proposed a heat transfer correlation for laminar convection in which the Nusselt number was simply a combination of the Nusselt numbers for laminar free and forced convection.

$$Nu^3_{mc} = Nu^3_{fc} + Nu^3_{nc} \text{ (uniform wall temperature)} \tag{2-9}$$

$$Nu^6_{mc} = Nu^6_{fc} + Nu^6_{nc} \text{ (uniform heat flux)} \tag{2-10}$$

This approach is quite effective as the Nusselt number reaches the proper limits when the flow approaches pure free and forced convection. As a result the laminar data collected from the experimental loop will be used to check these correlations.

The transition regime between laminar and turbulent flows has not been extensively explored in the past. There have been a few attempts to define this region, Kaupas et al. [1989], Tanaka et al. [1987], Kaupas and co-workers even proposed a heat transfer correlation based upon a combination of an "intermittency coefficient" and laminar and turbulent convection correlations. However these efforts are not sufficient to define the boundaries between the laminar and transitional regimes and transitional and turbulent regimes. One of the goals of this heat transfer experiment is to determine these boundaries and develop a correlation for this transition regime.

As opposed to the transition regime, the turbulent convection regime has been extensively studied over the last four decades. Correlations have been developed for turbulent mixed convection that account for the deterioration of heat transfer in buoyancy-aided convection. The

Nusselt number in this region is generally thought to be a function of Ra(Gr), Re, Bo*, K_v, and the distance-to-diameter ratio (z/D). The first four parameters are familiar as they were parameters determined most important in identifying convection regimes. The distance-to-diameter ratio is included because the flow is never fully developed in a buoyancy aided heated channel. One such correlation developed by Celata and co-workers [1998] appears to be the most promising. In their correlation they normalized the upflow mixed convection Nusselt number, $Nu_{m,up}$, by the Nusselt number for downflow, $Nu_{m,df}$, which, according to Churchill [1998], may be expressed as:

$$Nu^3_{m,df} = Nu^3_{fc} + Nu^3_{nc} \qquad\qquad (2\text{-}11)$$

They then correlated the normalized Nusselt number, Nu^*, for upflow with experimental data obtained from water. The final form of their correlation is:

$$Nu^* = Nu_{m,up}/Nu_{m,df} = F\,(Bo, L/D) \qquad\qquad (6\text{-}6)$$

where the Buoyancy parameter, Bo, is taken following Jackson, et al [1989], as:

$$Bo = 8 \times 10^4 \, Gr_q/(Re_f^{3.425} \, Pr_f^{0.8}) \qquad\qquad (6\text{-}7)$$

The above formulation has the advantage that Nu^* starts from a value of unity at Bo close to zero, i.e., no buoyancy effect, and again reaches a value of unity as Bo approaches infinity (or a very large value) where the buoyancy effect dominates. In addition, similar to the laminar region formulation proposed by Churchill [1998], the above formulation does not need to define the boundaries among the forced, mixed and the free convection regimes. The correlation is valid for all flow regimes in turbulent convection. However as the experiment was conducted for water the proposed experimental loop will be used to test the correlation for gases.

Finally in addition to identifying pre-existing heat transfer correlations, it is also important to determine where most of the experimental data concerning convection flow regimes has been taken and where there are significant gaps in the experimental data. The following table identifies the ranges of Re number where experimental data has been taken for convection flow

18

regimes. From Table 2-1 it is apparent that there exists a lack of experimental data for Re < 3000. This range of Re numbers encompasses both laminar flow and the transition regime between laminar and turbulent flows. While heat transfer correlations have been proposed for laminar convection they still must be verified experimentally. Accurate heat transfer correlations for the transitional regime may only be proposed after the regime has been clearly defined by experimental data.

Table 2-1 Parameters of various gas upflow experiments in heated tubes

	Shehata [1984]	Tanaka, et al [1987]	Kaupas, et al [1989, 1991]
Gas	Air	Nitrogen	Air
System Pressure (MPa)	~ 0.1	0.1 to 5.0	0.1 to 0.7
Tube I. D. (mm)	27.4	23.0	36.3
Heated length (mm)	823	2530	4295
Reynolds No. (at inlet)	4000 – 6000	3000 - 5200	3500 - 40000
Non-dimensional heat flux, q^+	0.0018 – 0.0045	(Not reported)	0.00035 – 0.00236

References

1. Aicher, T. and Martin, H., "New correlations for mixed turbulent natural and forced convection heat transfer in vertical tubes," *International Journal of Heat and Mass Transfer,* Vol. 40, No. 15, pp. 3617-3626, 1997.

2. Bankston, C. A., "The transition from turbulent to laminar gas flow in a heated pipe." *Journal of Heat Transfer*, Vol. 92, pp. 569-579, 1970.

3. Bejan, A, Convection Heat Transfer,, Chapter 4, John Wiley & Sons, Inc., 1993.

4. Burmeister, L. C., Convective Heat Transfer, 2nd Edition, Chapter 10 , John Wiley & Sons, Inc., 1993.

5. Celata, G. P., D'Annibale, F., Chiaradia, A., and Cumo, M., "Upflow turbulent mixed convection heat transfer in vertical pipes," *International Journal of Heat and Mass Transfer*, Vol. 41, pp. 4037-4054, 1998.

6. Churchill, S.W., "2.5.10 Combined free and forced convection in channels," Heat Exchanger Design Handbook, ed. Hewitt, G.F., Begell House, Inc., 1998.

7. Jackson, J. D., Cotton, M. A., and Axcell, B. P., "Studies of mixed convection in vertical tubes," *International Journal of Heat and Fluid Flow*, Vol. 10, No. 1, pp. 2-15, 1989.

8. Jackson, J. D., Personal Communication, April 1998 as referenced in Mikielewicz, D. P., et al, "Temperature, velocity and mean turbulence structure in strongly heated internal gas flows – Comparison of numerical predictions with data," International Journal of Heat and Mass Transfer, Vol.45, pp. 4333-4352, 2002.

9. Kaupas, V. E., Poskas, P. S., and Vilemas, J. V., "Heat Transfer to a Transition-Range Gas Flow in a Pipe at High Heat Fluxes" (2. Heat Transfer in Laminar to Turbulent Flow

Transition) and (3. Effect of Buoyancy on Local Heat Transfer in Forced Turbulent Flow), HEAT TRANSFER-Soviet Research, Vol. 21, No. 3. pp. 340-361, 1989.

10. Tanaka, H., Maruyama, S., and Hatano, S., "Combined forced and natural convection heat transfer for upward flow in a uniformly heated, vertical pipe," *International Journal of Heat and Mass Transfer,* Vol. 30, No. 1, pp. 165-174, 1987.

11. Parlatan, Y., "Friction Factor and Nusselt Number Behavior in Turbulent Mixed Convection in Vertical Pipes," Ph. D. Thesis, Department of Nuclear Engineering, MIT, June 1993.

3. EXPERIMENTAL LOOP DESIGN

The non-dimensional parameters used to characterize convection flow regimes, Ra, Re, Bo*, and K_v will serve as guidelines for the design of the experimental thermal-hydraulic loop. Initially the design focus will be on matching the ranges of each of the aforementioned non-dimensional parameters encountered in post-LOCA operation of the proposed GFR. Once this requirement is met the design focus will shift to expanding these ranges in order to provide experimental data for as many flow regimes mentioned in Table 1.1 as possible. Heat transfer in the proposed experimental loop will be analyzed using LOCA-COLA (Loss of Coolant Accident – COnvection Loop Analysis), a computer code developed at MIT. LOCA-COLA was originally developed to analyze decay heat removal by natural circulation in the GFR core. However the code is sufficiently flexible to model a variety of thermal-hydraulic loops. A detailed description of LOCA-COLA and its FORTRAN coding is given by Williams et al. [2003]

3.1 GFR LOCA-COLA Analysis

Several possible GFR block-core designs and operating conditions are described in Appendix A. An analysis of the decay heat removal for these various core designs and operating conditions was conducted at MIT using LOCA-COLA. [Williams et al. 2003] Figures 3-1, 3-2, and 3-3 are graphs of the four relevant non-dimensional parameters for convection, Ra, Re, Bo*, and K_v, measured along a core channel from inlet to outlet for the various geometries and operating conditions of the GFR. As expected, the GFR operates predominantly in a mixed convection regime following a LOCA (Figure 3-1). Perhaps more importantly, Figure 3-1 also shows that the GFR will operate in the transition regime between laminar and turbulent mixed convection and mixed and forced convection. As mentioned in the previous chapter, the transition between forced and mixed convection is characterized by the onset of buoyancy-aided convection. Figure 3-2 is evidence of this fact as it shows that a significant portion of the turbulent flow encountered in the GFR loop will experience the onset of buoyancy-influenced convection. As a result it is important for the experimental loop to be able to generate data both above and below the onset of buoyancy-influenced convection. Finally it is apparent from Figure 3-3 that the turbulent flows

of the GFR loop will not exhibit lower heat transfer characteristics due to laminarization of the flow. As a result operation of turbulent flow regimes where laminarization is prominent should be avoided in the experimental loop in order to reproduce the heat transfer characteristics of the GFR loop.
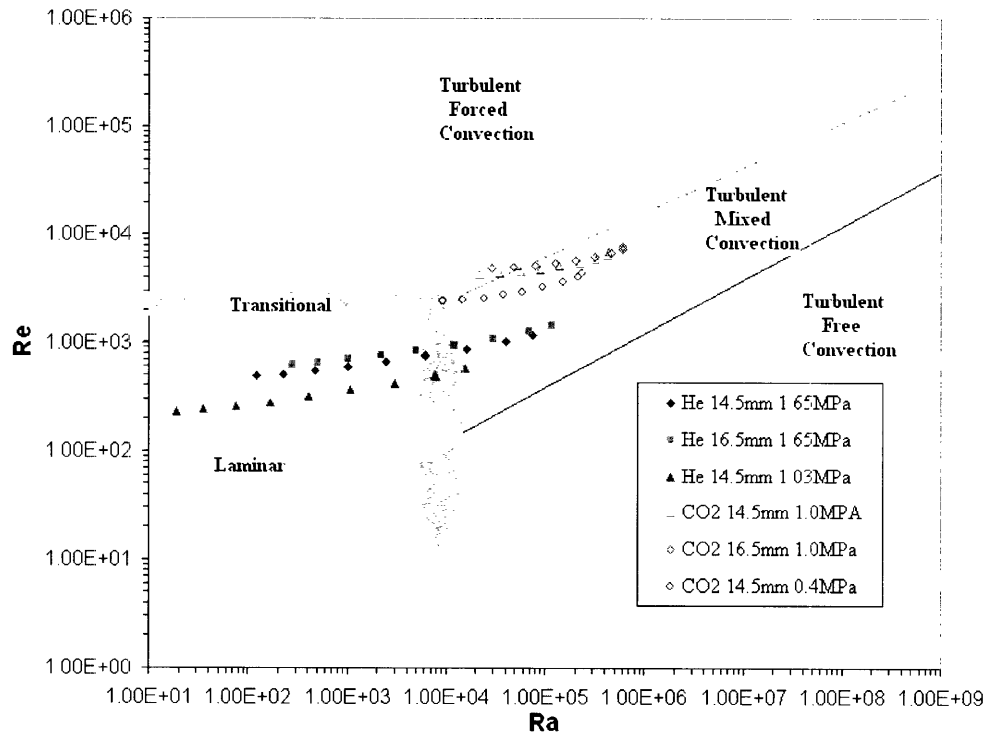
Figure 3-1 Ra vs. Re map for reactor prototype loop
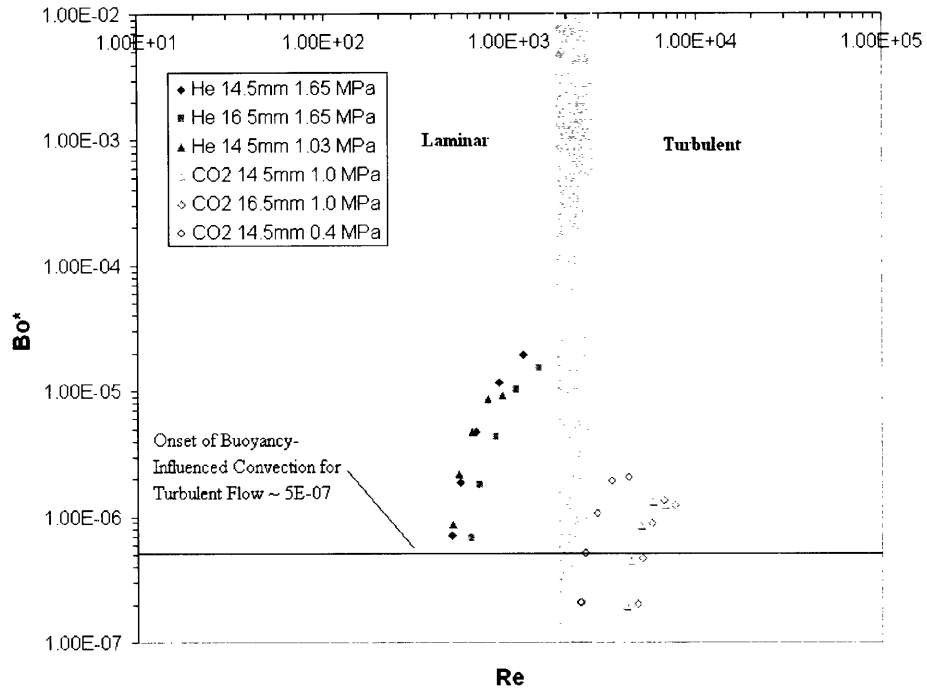
Figure 3-2 Buoyancy parameter for reactor prototype loop
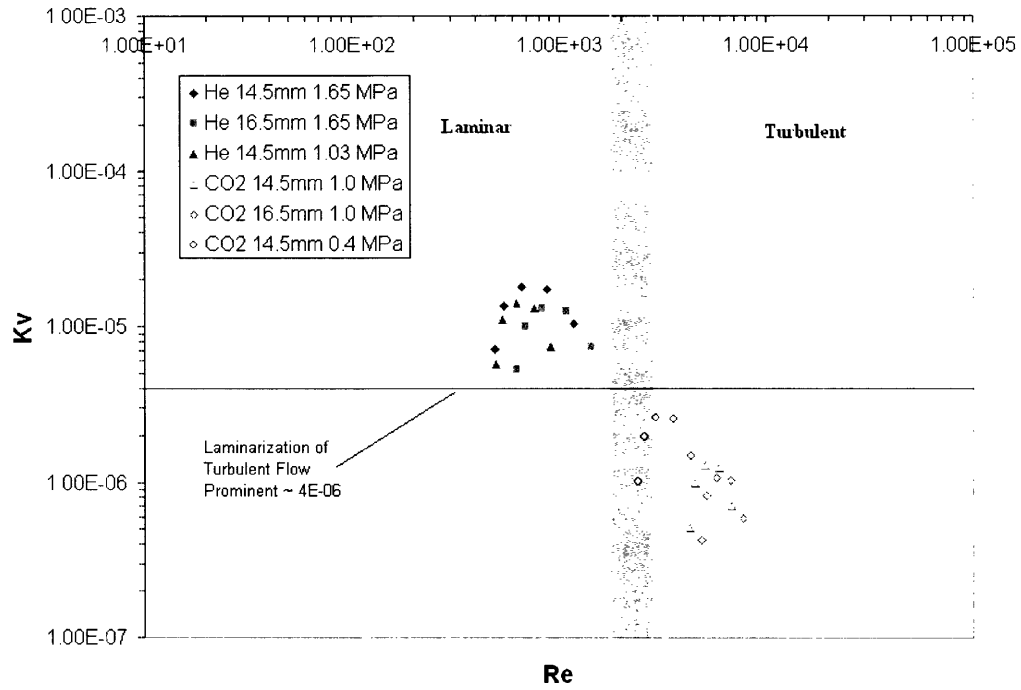
Figure 3-3 Acceleration parameter for reactor prototype loop

24

3.2 Experimental Loop Design

As mentioned previously, the experimental loop was designed with two objectives in mind, the first being to encompass the entire range of post-LOCA operating conditions as depicted in Figures 3-1, 3-2, and 3-3, while the second being to encompass as many of the flow regimes portrayed in Table 1.1 as possible. In addition to filling in experimental gaps in convection flow regimes the second objective will allow the heat transfer analysis to be extended into flow regimes where heat transfer correlations are well established, i.e. turbulent and laminar forced convection. As a result, we will be able to benchmark some of our data and resulting heat transfer correlations with those found in the literature.

3.2.1 Design Considerations and Constraints

We were initially faced with several considerations when contemplating the design for the experimental loop. First we wanted to keep a certain degree of similitude between the geometry of the GFR (prototype) loop and the experimental loop, as key non-dimensional parameters such as Ra and Re number are dependent upon the hydraulic diameter (inner diameter of the tube). As a result a test section diameter of 16mm and length of 2m was chosen to closely match the prototype loop (For GFR geometry see Appendix A). Secondly, since most of the experimental runs may utilize natural circulation, we wanted to maximize the available driving force from this source. To this end, the thermal elevation difference between the heated channel and the heat exchanger was set at a maximum value of 4.25m (limited by the height of the lab space available).

Another main design consideration for the loop resulted from the addition of a hot-wire probe for measuring local fluid velocity and temperature profiles in the heated test section. Accurate calibration of this hot-wire probe above 450°C is extremely difficult. As a result the maximum bulk fluid temperature for the heated test section will be restricted to 450°C. This constraint is actually very significant as the coolant flow in the GFR prototype is greater than 1000°C for some cases. And since non-dimensional scaling parameters for convection flow regimes are dependent upon temperature, we will have to compensate for the reduced operating

temperature of the experimental loop. The presence of the probe also leads to one more design modification. An extra heated test section with a diameter of 32mm was incorporated into the loop design, as a larger test section diameter will result in more accurate probe data. However this extra test section, with a hydraulic diameter twice that of the original test section, will also serve to increase the range of non-dimensional parameters encompassed by the experimental loop. The two heated test sections will be interchanged depending upon whether accurate prototype representation or probe data is desired.

One more constraint for the bulk fluid temperature arises from the fact that the experimental loop will incorporate a blower in order to reach forced convection regimes. The blower will be located in the cold leg of the experimental loop and will limit the maximum temperature of the fluid in the cold leg to 100°C as the rubber gaskets of the blower cannot exceed that temperature. Finally, the wall temperature in the heated test section is limited to 650°C to meet ASME code requirements at the maximum system pressure of 1.0 MPa for stainless steel 316.

3.2.2 Loop Description

Based upon the aforementioned design considerations, we arrived at the experimental loop depicted in Figure 3-4. The relevant component dimensions and descriptions are listed in Table 3.1. The overall dimensions of the loop are 7m high by 1m wide with 25.4mm ID tubing, the thermal elevation difference is 4.25m, the heated section of the loop is 2m long with either an ID of 16 or 32mm, and the heat exchanger has a length of 2m and a height of 1m. The heat exchanger length of 2 meters was calculated based upon counter flow with a constant wall temperature of 27°C. Stainless Steel 316 was the material of choice for the loop as it is relatively inexpensive and met ASME requirements at maximum system pressure and temperature.
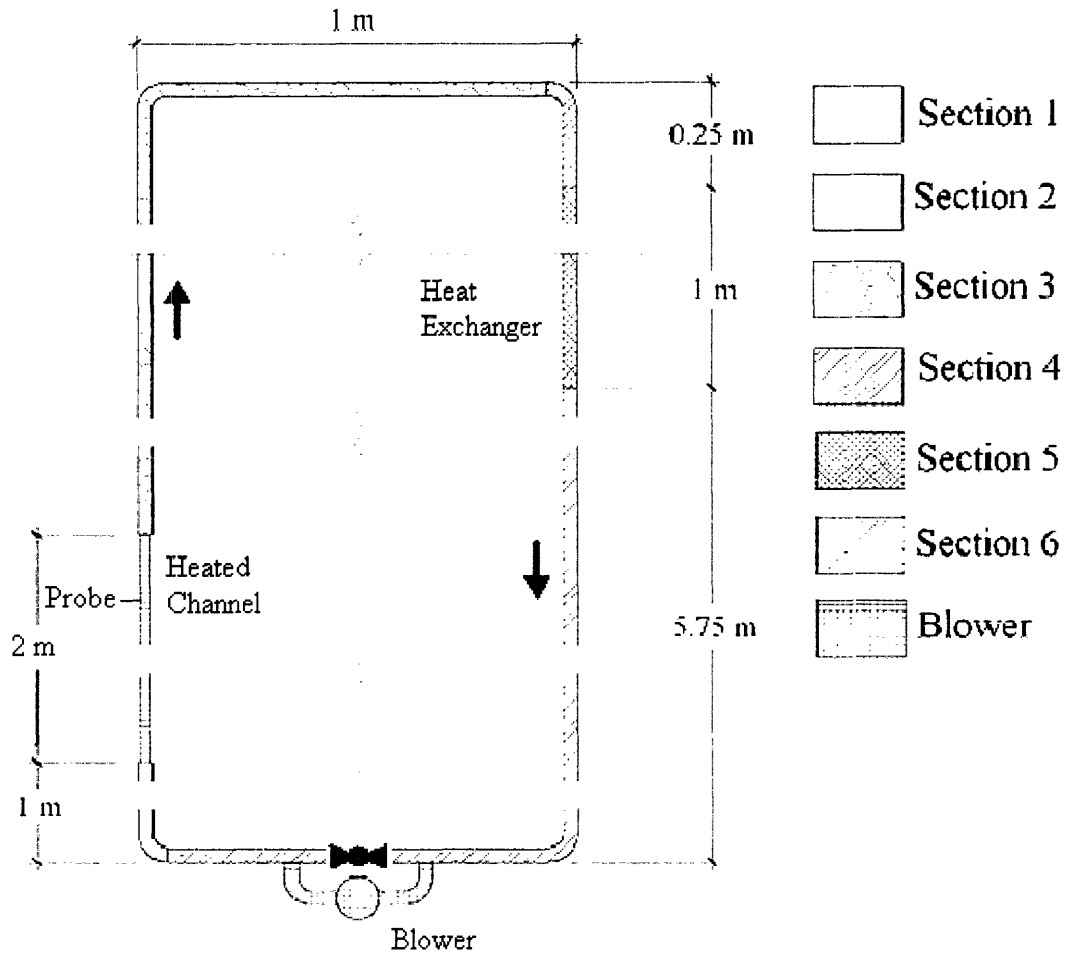
Figure 3-4 Experimental loop diagram

Table 3-1 Component description of experimental loop

Section	Description	Diameter	Material	ΔZ	Length
1	Upcomer	25.4 mm	SS 316	1.00 m	1.00 m
2	Heated CH.	16,32 mm	SS 316	2.00 m	2.00 m
3	Hot Leg	25.4 mm	SS 316	4.00 m	5.00 m
4	Downcomer	25.4 mm	SS 316	0.25 m	0.25 m
5	Heat Ex.	Tube in Tube	Cu	1.00 m	2.00 m
6	Cold Leg	25.4 mm	SS 316	5.75 m	6.75 m

27

3.3 LOCA-COLA Analysis of Proposed Experimental Loop

Having established the key dimensions of the experimental loop for input into LOCA-COLA, the next step is to determine the maximum range of non-dimensional convection parameters the loop can generate. This will be accomplished by running LOCA-COLA simulations utilizing both the 16mm and 32mm diameter test sections along with three gases, helium, nitrogen, and carbon dioxide, with pressures ranging from 0.1 MPa to 1.0 MPa.

3.3.1 Helium Trial Calculations

Six trials were conducted using helium as the test fluid with the variables being test section diameter and system pressure. For each trial the heat flux was adjusted to approach the maximum fluid bulk temperature of ~450 °C. Also for every trial the heat exchanger had a constant wall temperature of 27°C. Table 3.2 contains the three main inputs for the trials; test section diameter, system pressure, and heat flux, along with the resulting output loop parameters for each trial.

Table 3-2 LOCACOLA inputs and resulting parameters for He coolant

ID	Pressure	Heat Flux	Tin	Tout	Twall Max	Flow Rate	Pressure Drop	Total Heat	Velocity*	Re*
mm	MPa	kW/m^2	C	C	C	kg/s	Pa	kW	m/s	
16.0	0.2	0.50	27	456	457	2.25E-05	9.16	0.050	0.49	63
16.0	0.6	4.00	29	443	490	1.87E-04	25.90	0.402	1.37	529
16.0	1.0	8.00	47	411	512	4.25E-04	36.30	0.804	1.92	1210
32.0	0.2	0.45	27	435	441	4.27E-05	8.99	0.091	0.23	61
32.0	0.6	3.00	40	411	476	3.14E-04	22.20	0.603	0.58	449
32.0	1.0	5.50	73	409	521	6.34E-04	30.50	1.110	0.75	887

*Denotes average value in heated section

3.3.1.1 Scaling Ra number

As stated previously the main concern in scaling the Ra numbers between the prototype and model is the fact that the much higher temperatures of the prototype allow for a lower range of Gr numbers which in turn leads to lower Ra numbers. However looking at Figure 3-5 we see that

with helium the model loop is able to generate a range of Ra numbers from 1×10^1 to 1×10^6 which completely encompasses the range of Ra numbers found for the prototype. If we look a little closer at Figure 3-5 we see that the two trials conducted at 0.2 MPa generate the lowest ranges of Ra numbers. Now besides the fact that these two trials were conducted at the same system pressure they have one other important similarity, a very small temperature difference between the maximum wall temperature and bulk fluid exit temperature. For the 16 mm test section at 0.2 MPa this difference is only 1 °C, and for the 32 mm test section at 0.2 MPa this difference is only 6 °C. (For helium in the prototype this difference is ~100 °C) This latter similarity is the reason why the 0.2 MPa cases can generate lower Ra number ranges as the Gr number is proportional to the difference between the temperature of the wall and the bulk fluid temperature, (T_w-T_b).
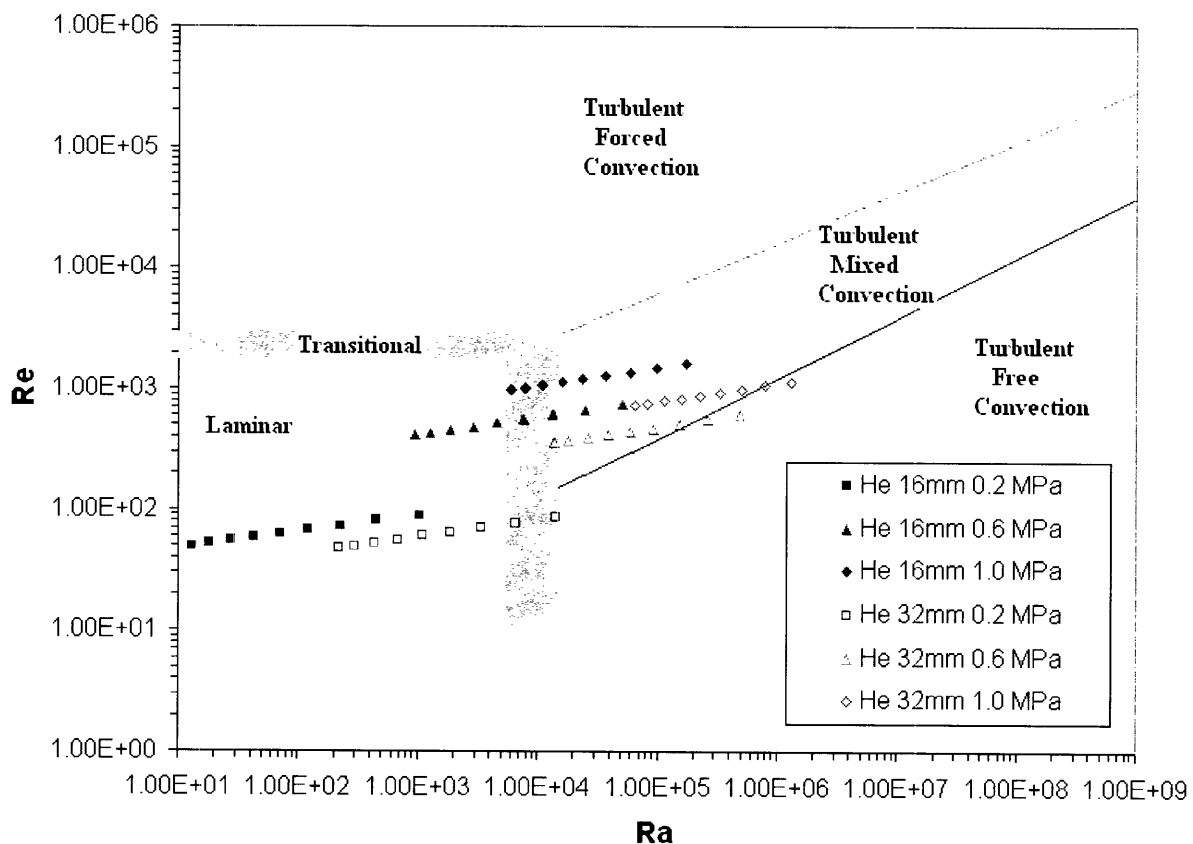
Figure 3-5 Ra vs. Re map for experimental loop with He coolant

3.3.1.2 Scaling Bo* number

The Buoyancy parameter is important for its influence upon convection. According to Jackson [1989], buoyancy-influenced turbulent convection in round tubes occurs when Bo* ~ 5 x 10^{-7}. This is important as the prototype Bo* number range of 2 x 10^{-7} to 3 x 10^{-5} includes this value for the onset of buoyancy-influenced turbulent convection. However, looking at Figure 3-6, we see that buoyancy-influenced turbulent convection is irrelevant in the helium trial calculations as the flow is laminar for every case. As a result, we will look to nitrogen and carbon dioxide to generate turbulent flows, where buoyancy-influenced convection is relevant.
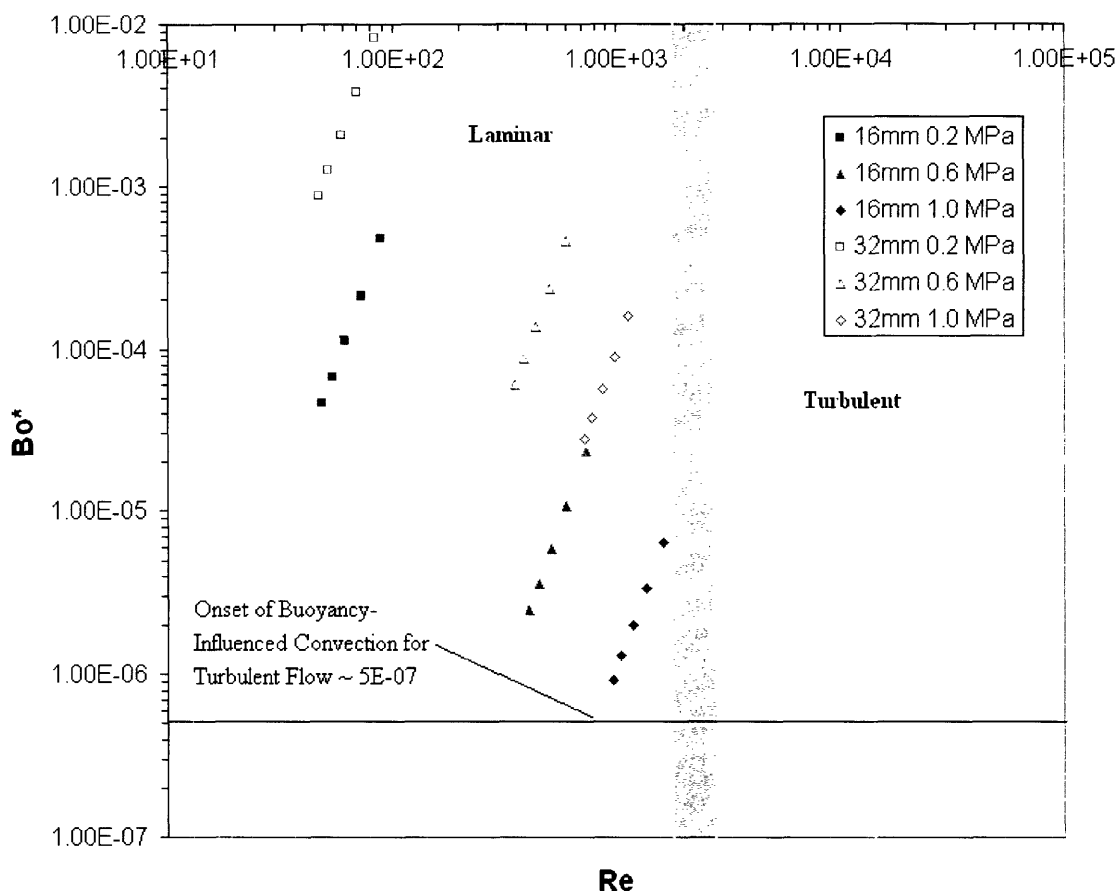
Figure 3-6 Buoyancy parameter for experimental loop with helium coolant

3.3.1.3 Scaling K_v parameter

As stated in Chapter 2, the acceleration parameter is important in determining if laminarization is likely to occur in turbulent flow. As per McEligot and Jackson [2004], laminarization is prominent at $K_v \sim 4 \times 10^{-6}$. On the other hand, laminarization is unimportant when $K_v < 1 \times 10^{-6}$. However, as stated previously, all of the helium trial calculations resulted in laminar flow where the process of laminarization is not relevant. As a result the acceleration parameter is simply representative of the acceleration of the gas flow and is plotted here for completeness. Figure 3-7 shows that helium will operate in a K_v range of 4×10^{-6} to 3×10^{-4}.
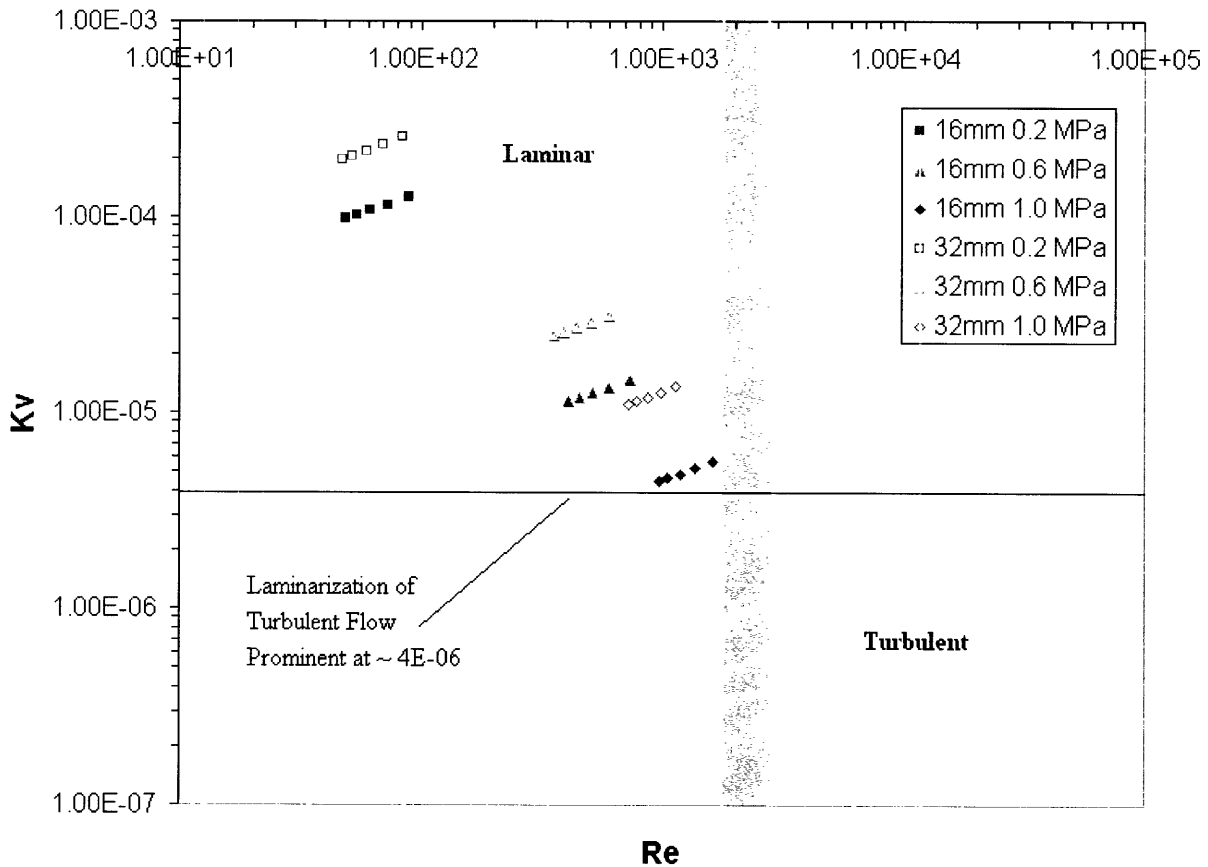
Figure 3-7 Acceleration parameter for experimental loop with helium coolant

3.3.2 Nitrogen Trial Calculations

The experimental setup for nitrogen is very similar to that of helium, namely the same input parameters and constraints were considered. However, since the area of overlap between the relevant non-dimensional parameters of the two coolants occurs at higher helium pressures and lower nitrogen pressures, the system pressure for the nitrogen coolant was extended down to 0.1 MPa for both the 16 and 32 mm test sections to create a larger overlap. As a result we will be able to compare heat transfer correlations developed from the two coolants for a larger flow regime area. However it should be noted that for 5 out of the total 8 trials the inlet temperature of the test section is greater than 100°C, which violates the maximum temperature for the rubber gaskets of the blower. This problem is easily solved as the inlet temperatures of the test section can be brought below 100°C by simply increasing the length of the heat exchanger.

Table 3-3 LOCACOLA inputs and resulting parameters for N2 coolant

ID	Pressure	Heat Flux	Tin	Tout	Twall Max	Flow Rate	Pressure Drop	Total Heat	Velocity*	Re*
Mm	MPa	kW/m^2	C	C	C	kg/s	Pa	kW	m/s	
16.0	0.1	1.10	37	446	521	2.54E-04	28.70	0.111	1.62	773
16.0	0.2	2.50	79	435	611	6.62E-04	43.30	0.251	2.29	1970
16.0	0.6	5.50	130	428	565	1.73E-03	94.00	0.553	2.18	4980
16.0	1.0	8.00	157	435	557	2.69E-03	134.00	0.804	2.13	7560
32.0	0.1	0.80	58	440	534	3.96E-04	24.80	0.161	0.66	595
32.0	0.2	1.50	113	414	572	9.40E-04	33.80	0.302	0.86	1380
32.0	0.6	3.00	161	406	620	2.30E-03	73.10	0.603	0.75	3280
32.0	1.0	4.55	174	398	661	3.81E-03	108.00	0.915	0.76	5410

*Denotes average value in heated section

3.3.2.1 Scaling Ra number

It is apparent from Figure 3-8 that the model utilizing nitrogen cannot cover the lower portion of the prototype Ra number range. However nitrogen does provide an overlap of Ra numbers between itself and helium from 1×10^3 to 1×10^6, which will prove useful for future comparisons. Furthermore the use of nitrogen as a coolant allows us to extend the operating range of the loop further into turbulent mixed convection and even across the boundary between mixed and free convection. This is important as data taken from the transition region between

mixed and free convection may be used to verify the boundary between mixed and free
convection proposed by Burmeister [1993].
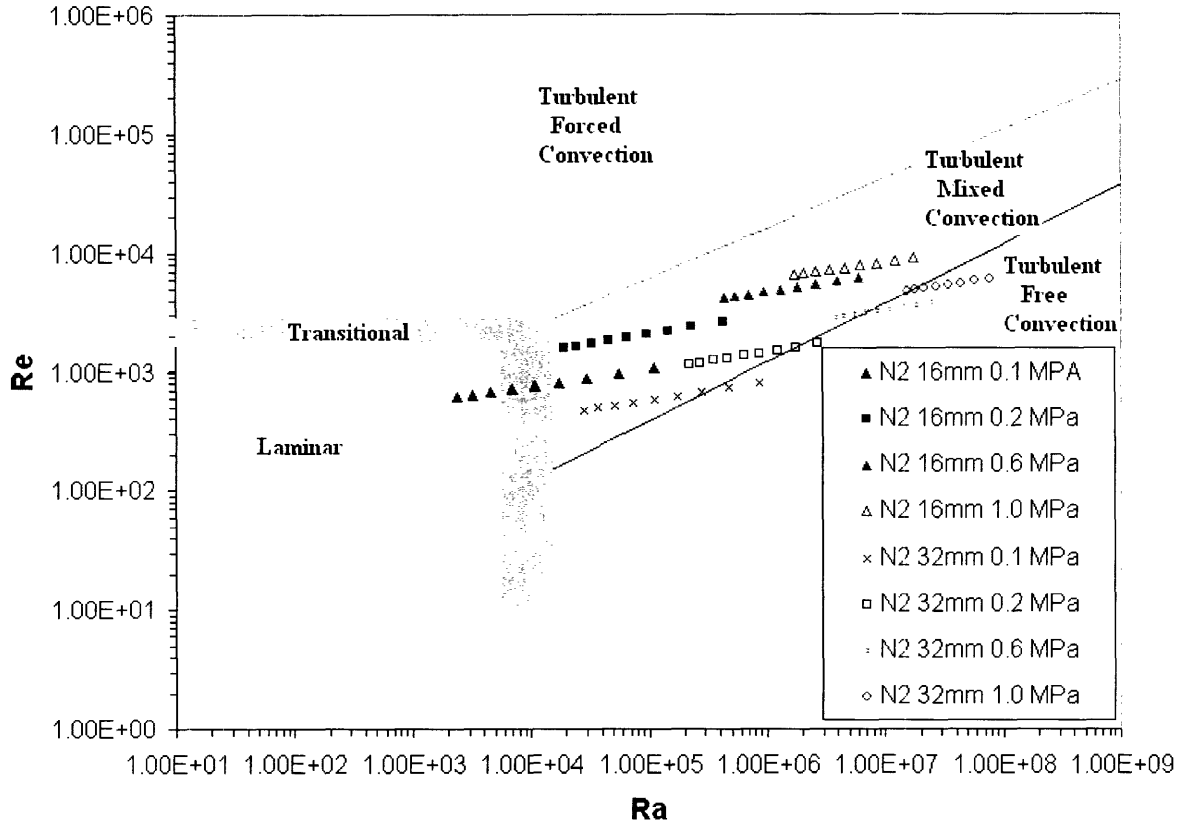
Figure 3-8 Ra vs. Re map for experimental loop with nitrogen coolant

3.3.2.2 Scaling Bo* number

As mentioned in section 3.3.1.2 an important Bo* number is approximately 5×10^{-7} as it signals
the onset of buoyancy-influenced convection in turbulent flow. Also, as mentioned previously
the model loop utilizing helium was unable to generate Bo* numbers this low. However, when
the coolant in question is nitrogen the Bo* number range is approximately 4×10^{-7} to 4×10^{-4}, as
shown in Figure 3-9. As a result we should be able to observe the onset of buoyancy-influenced
convection for turbulent flow in the model loop (boundary between forced and mixed
convection).
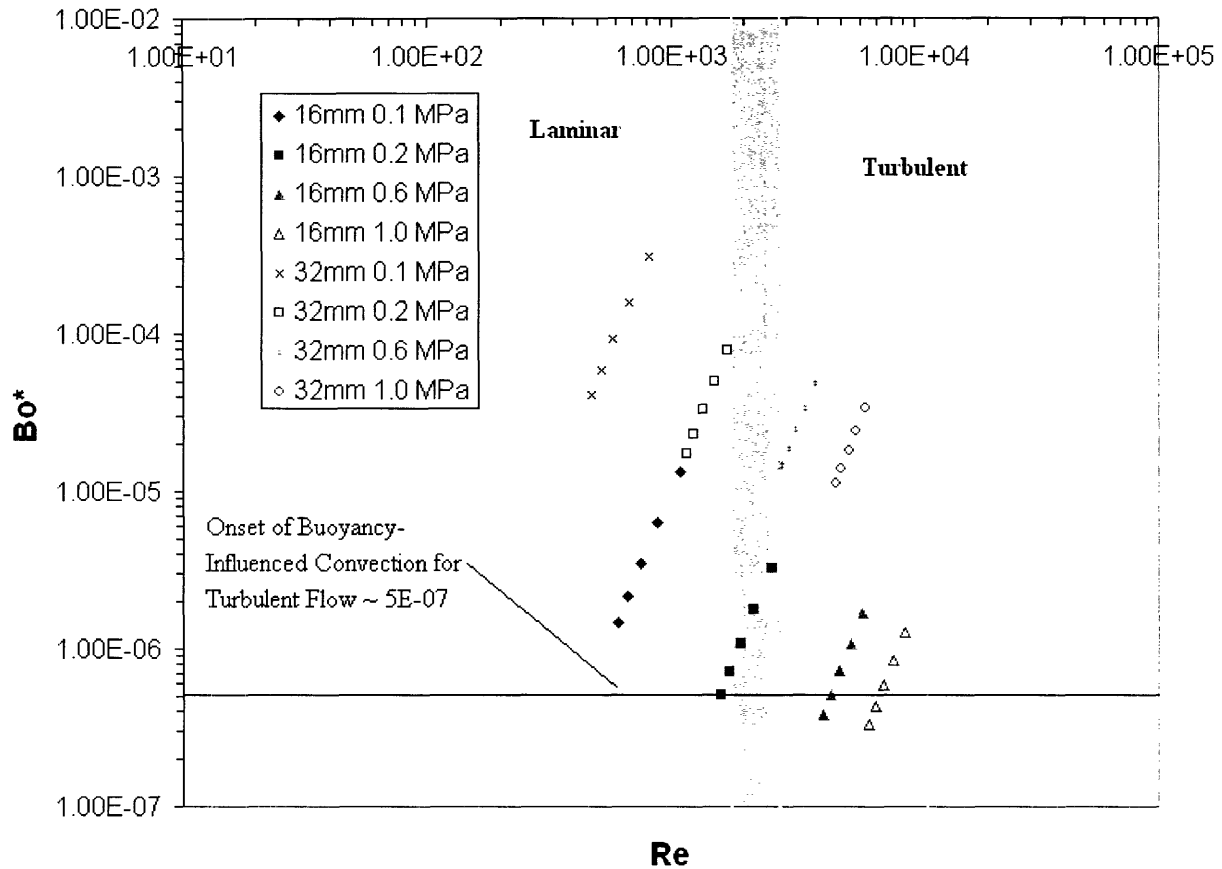
Figure 3-9 Buoyancy parameter for experimental loop with nitrogen coolant

3.3.2.3 Scaling K_v number

From Figure 3-10 we see that the model loop utilizing a nitrogen coolant is able to extend the K_v range covered by helium down to approximately 5×10^{-7}. As a result, the range of K_v numbers encompassed by the loop utilizing nitrogen as a coolant completely encompasses the transition region from where laminarization goes from being unimportant to being prominent, 5×10^{-7} to 4×10^{-6}. However, as was mentioned previously, the process of laminarization is only important when the flow is turbulent, i.e., the Re number is greater than ~2300. But while the K_v values above the threshold value of 4×10^{-6} occur for laminar flow they are sufficiently close to the transitional region between laminar and turbulent flow to merit close attention.

34
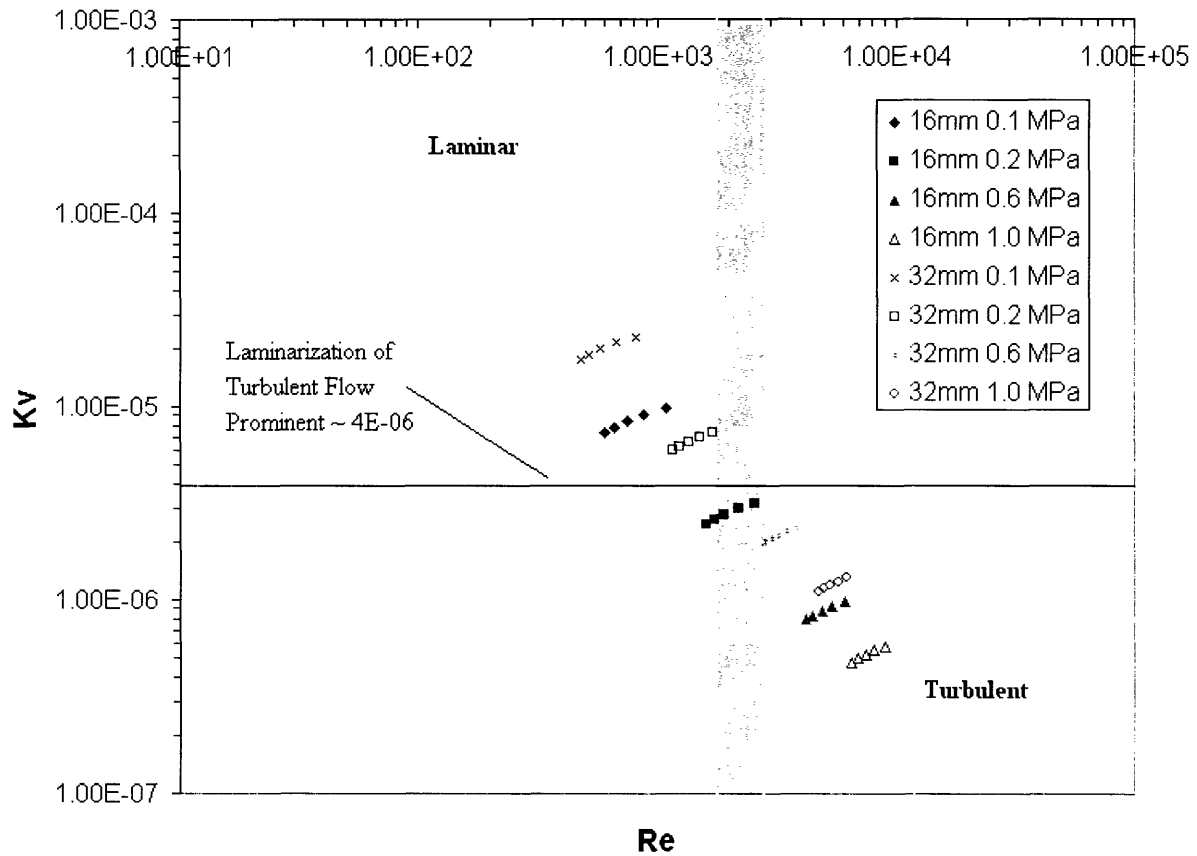
Figure 3-10 Acceleration parameter for experimental loop with nitrogen coolant

3.3.3 Carbon Dioxide Trial Calculations

The carbon dioxide trials, like the nitrogen trials, utilized a lower system pressure, 0.1 MPa, to provide for a larger area of overlap between the coolants. However, in this case lowering the pressure turns out to be even more effective as we can now compare heat transfer correlations developed from three different coolants for the same flow regimes.

Table 3-4 LOCACOLA inputs and resulting parameters for CO2 coolant

ID	Pressure	Heat Flux	Tin	Tout	Twall Max	Flow Rate	Pressure Drop	Total Heat	Velocity*	Re*
Mm	MPa	kW/m^2	C	C	C	kg/s	Pa	kW	m/s	
16.0	0.1	2.10	68	485	623	4.88E-04	39.30	0.211	2.15	1500
16.0	0.2	3.25	103	419	632	1.00E-03	58.00	0.327	2.28	3160
16.0	0.6	7.00	151	409	517	2.60E-03	127.00	0.704	2.12	7960
16.0	1.0	10.00	177	406	511	4.14E-03	178.00	1.005	2.09	12500
32.0	0.1	1.20	101	423	557	7.25E-04	29.50	0.241	0.83	1140
32.0	0.2	2.00	140	418	601	1.38E-03	45.80	0.402	0.84	2120
32.0	0.6	4.20	177	397	647	3.63E-03	102.00	0.845	0.76	5490
32.0	1.0	7.80	166	387	627	6.74E-03	180.00	1.568	0.83	10400

*Denotes average value in heated section

3.3.3.1 Scaling Ra number

Carbon dioxide as a coolant in the model loop serves a similar function as the nitrogen coolant. Namely it allows us to compare results between more than one coolant for the same Ra number and it also allows us to extend the range of Ra numbers encompassed by the model loop. (Figure 3-11) More specifically we will be able to compare results from all three coolant fluids for a Ra number range of approximately 1×10^4 to 1×10^6, and a Re number range of roughly 1000-2000. The carbon dioxide trials also allow us to obtain more data for the transition from mixed to free turbulent convection.
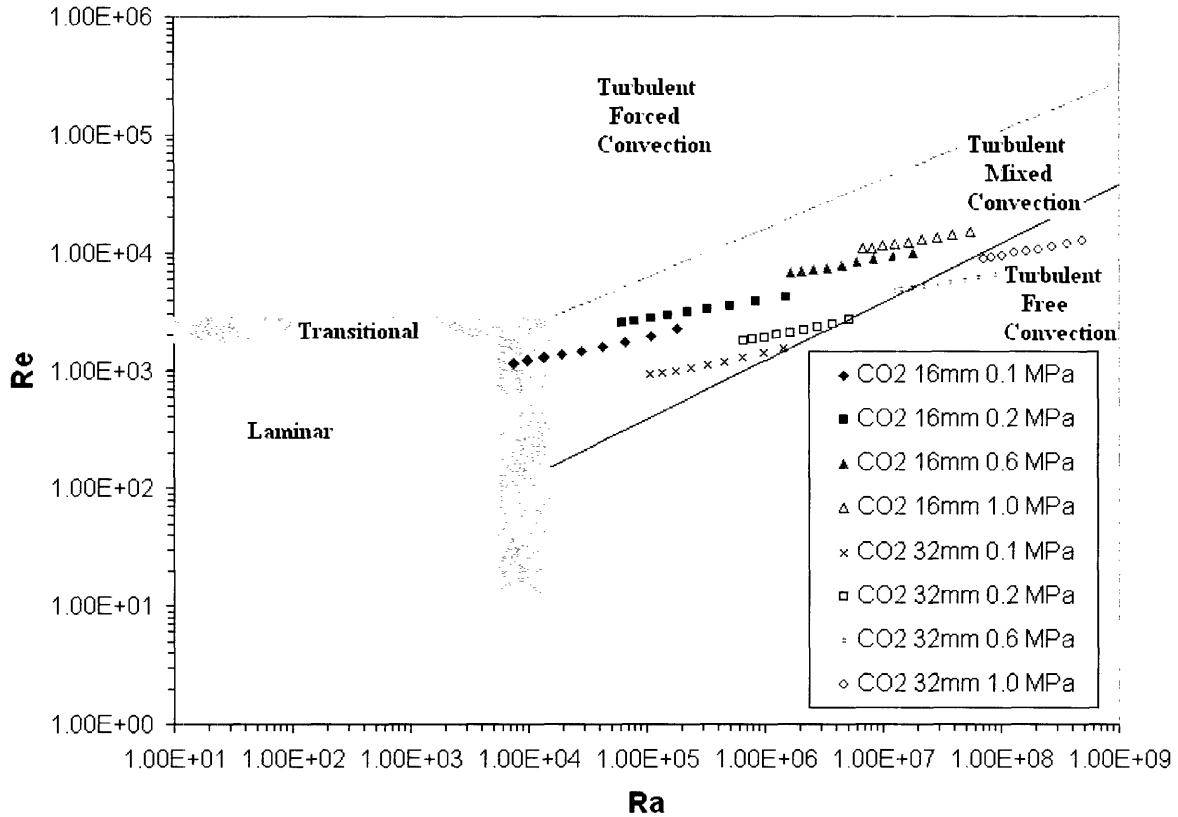
Figure 3-11 Ra vs. Re map for experimental loop with carbon dioxide coolant

Chart axis labels and legend:

Y-axis (Re): 1.00E+06, 1.00E+05, 1.00E+04, 1.00E+03, 1.00E+02, 1.00E+01, 1.00E+00

X-axis (Ra): 1.00E+01 1.00E+02 1.00E+03 1.00E+04 1.00E+05 1.00E+06 1.00E+07 1.00E+08 1.00E+09

Regions: Turbulent Forced Convection; Turbulent Mixed Convection; Turbulent Free Convection; Transitional; Laminar

Legend:
- CO2 16mm 0.1 MPa
- CO2 16mm 0.2 MPa
- CO2 16mm 0.6 MPa
- CO2 16mm 1.0 MPa
- CO2 32mm 0.1 MPa
- CO2 32mm 0.2 MPa
- CO2 32mm 0.6 MPa
- CO2 32mm 1.0 MPa

3.3.3.2 Scaling Bo* number

Since we have already established the fact that we can encompass the regime of buoyancy-influenced convection, the only objective left is to extend the model loop Bo* to lower values in order to encompass more of the prototype Bo* range of 2×10^{-7} to 3×10^{-5}, i.e., dominant forced convection. Figure 3-12 shows that the lowest possible Bo* number obtained in the model loop utilizing the carbon dioxide coolant is approximately 2.5×10^{-7}, and while the prototype Bo* range extends to a slightly lower value, the difference is negligible.

37
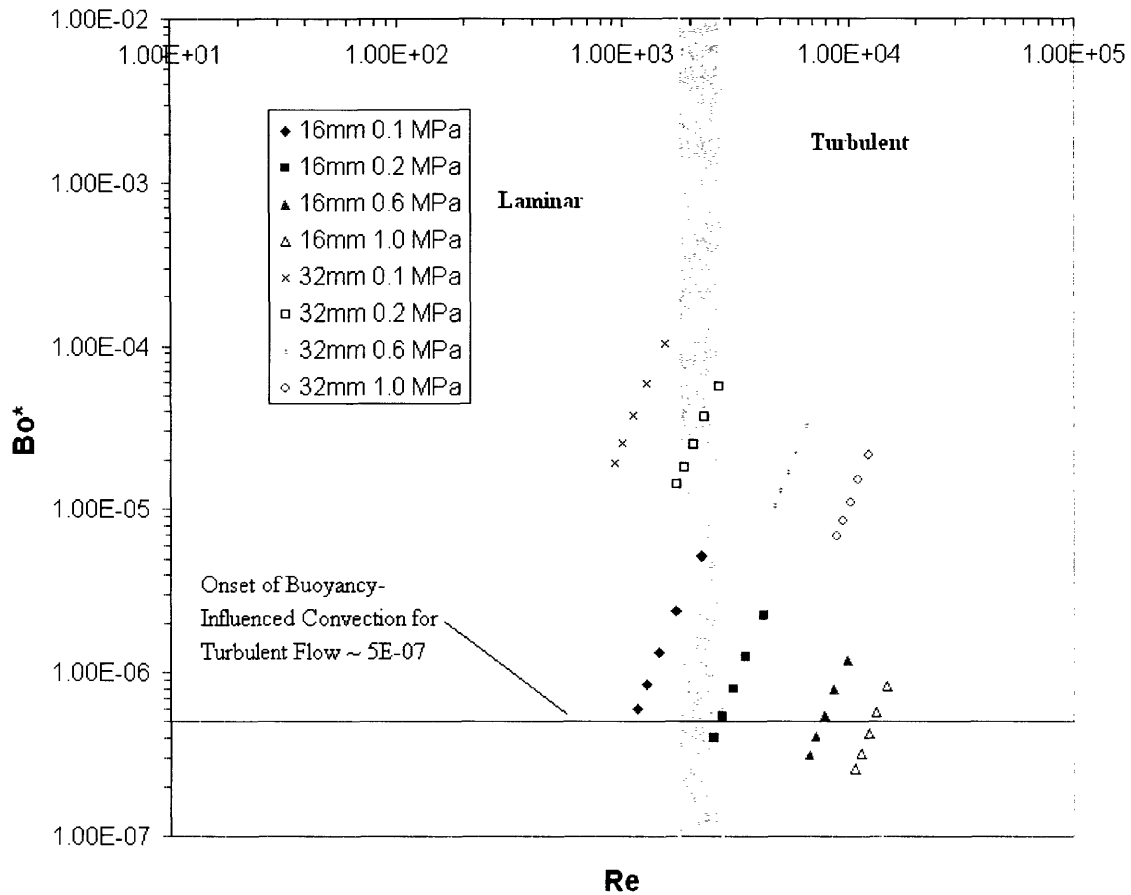
Figure 3-12 Buoyancy parameter for experimental loop with carbon dioxide coolant

3.3.3.3 Scaling K_v number

The carbon dioxide trials pose the most difficulty in avoiding laminarization of turbulent flow in the mixed convection regimes. Looking at Figure 3-13 we see that the trial runs operating in the transition region between laminar and turbulent flow have K_v values greater than 4×10^{-6}. Whether laminarization in this transition region is important or not will have to be determined experimentally.
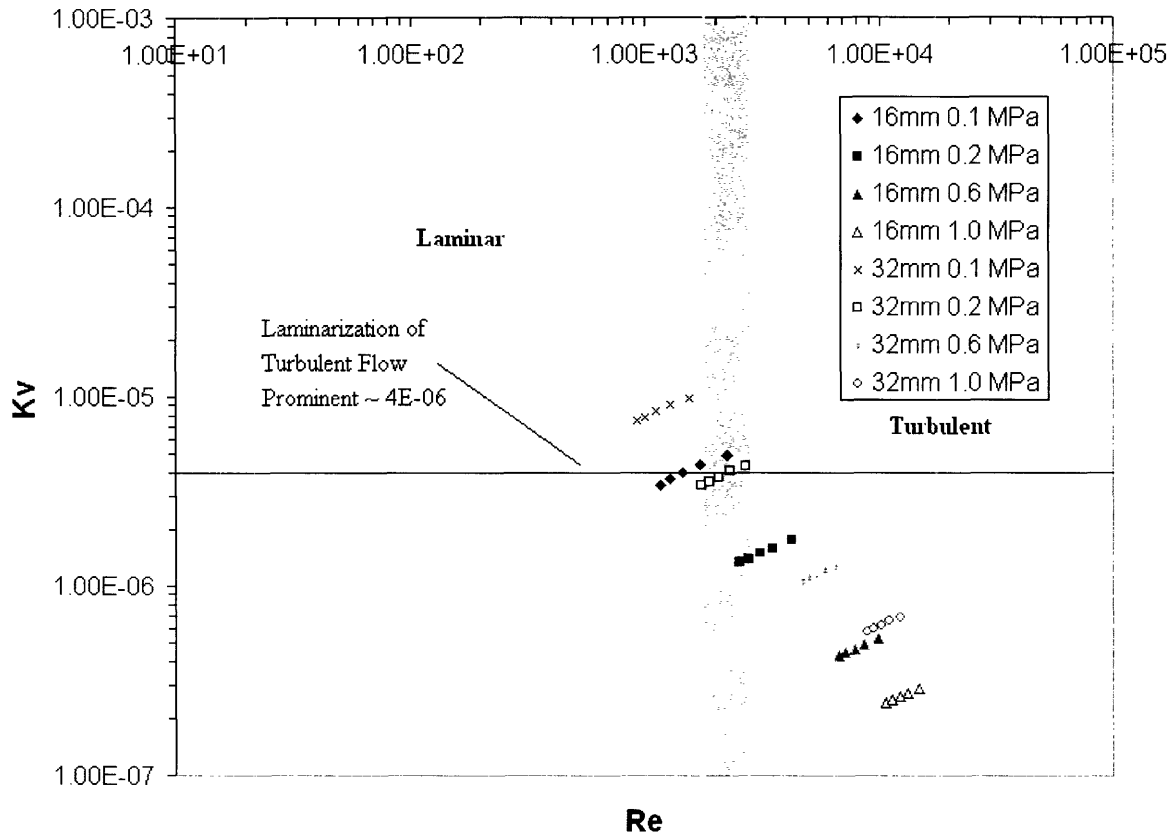
Figure 3-13 Acceleration parameter for experimental loop with carbon dioxide coolant

3.3.4 Trials Utilizing the Blower

While we were able to completely map the mixed convection region of the GFR conditions using our various input parameters under the guiding force of natural circulation, we would like to be able to generate data from both laminar and turbulent forced convection regimes in order to compare with accepted heat transfer correlations and analyses for the aforementioned regimes. Furthermore we will only utilize helium for these trials as the nitrogen and carbon dioxide coolants would require much more heat input to reach turbulent-forced convection. As the onset of turbulent flow occurs at a Re number of approximately 2300, we will need to generate data both significantly below and above this number for comparison to accepted results. Figure 3-14 is a Ra vs. Re map for helium coolant utilizing the blower. From the figure we can see that at a pressure of 0.1MPa with 1.1 KW deposited in the flow we can generate a laminar forced convection regime with a Re number range of approximately 1000-1900. And as we increase the

pressure and power we can generate a turbulent forced convection regime with a Re number range of approximately 4000-10000.
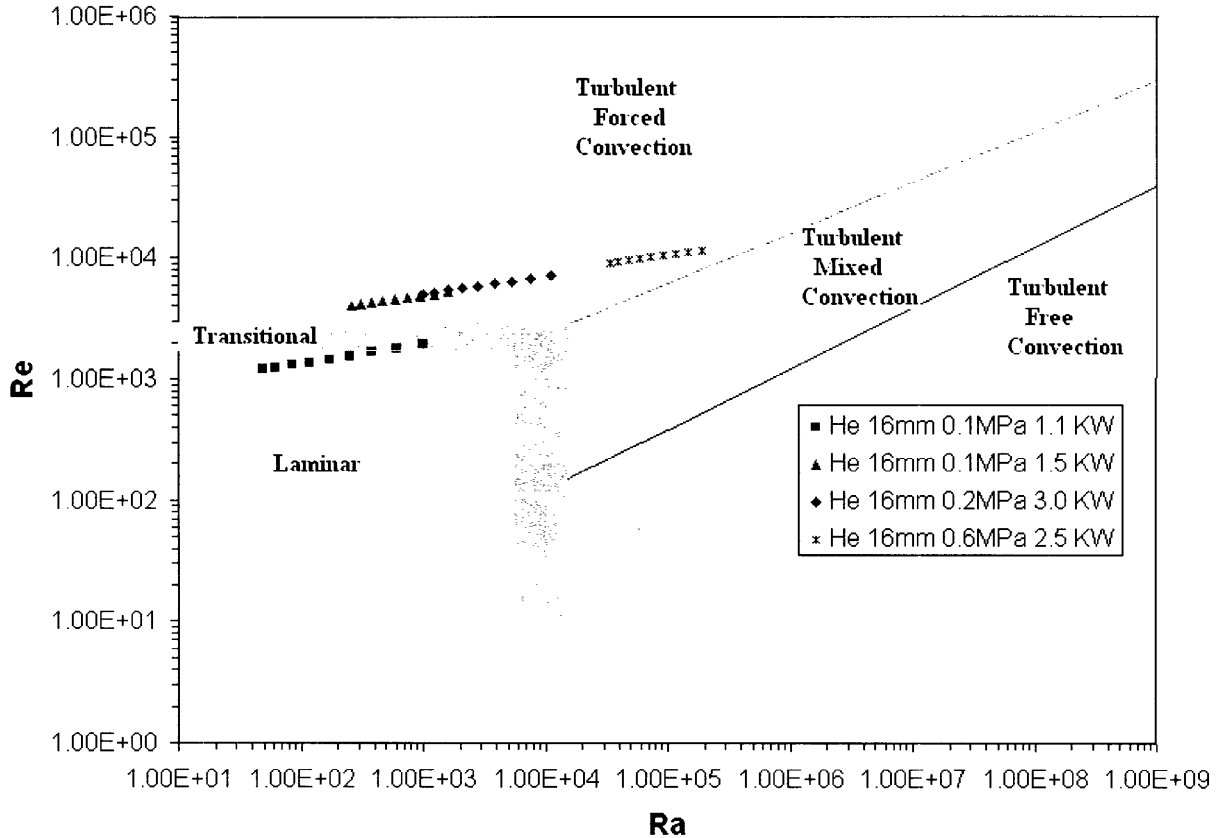
Figure 3-14 Turbulent and laminar forced convection for experimental loop with He coolant

3.4 LOCA-COLA Analysis Summary

In the preceding sections it has been shown that through the use of three fluids, helium, nitrogen, and carbon dioxide, two test section diameters, 16 and 32 mm, and varying system pressures, 0.1 MPa-1.0 MPa, that the relevant dimensionless parameters, Ra, Re, K_v , and Bo* can be conserved from the GFR prototype to the experimental model. Figures 3-15, 3-16, and 3-17 are graphs of the entire ranges of the Ra, Re, K_v , and Bo* numbers resulting from natural circulation for both the prototype and model. Furthermore in addition to covering the entire range of reactor conditions our second objective was to encompass as many of the nine flow and heat transfer regimes mentioned in Table 1.1 From Figure 3-15 it is apparent that we can cover laminar, transitional, and turbulent mixed convection flows. And since we can also control the

Re number through use of the blower we should be able to operate in mixed and forced convection for laminar, transitional, and turbulent flows. Figures 3-16 and 3-17 act, respectively, as guidelines to determine whether buoyancy-influenced convection and/or laminarization effects are likely to be important. As a result using the experimental loop we should be able to develop heat transfer correlations that are not only applicable to the GFR prototype loop but to a larger range of flow and convection regimes.
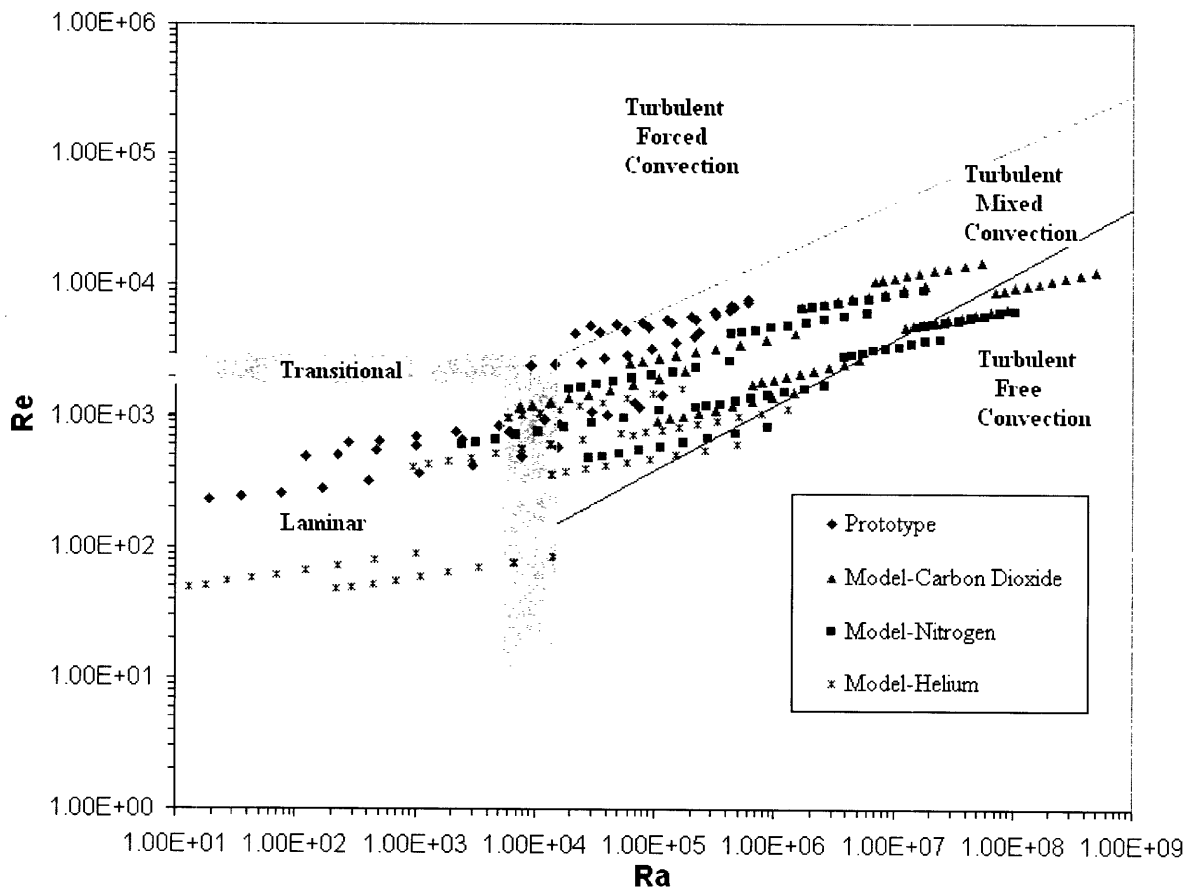
Figure 3-15 Complete Ra vs. Re map generated from experimental loop
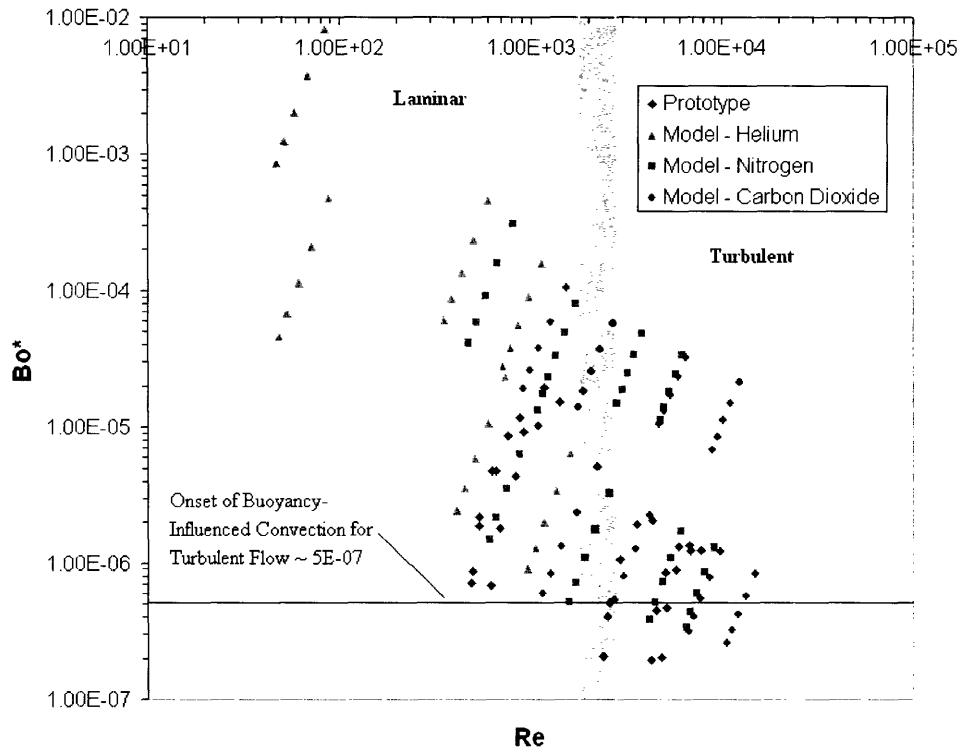
Figure 3-16 Range of Buoyancy parameter generated from experimental loop
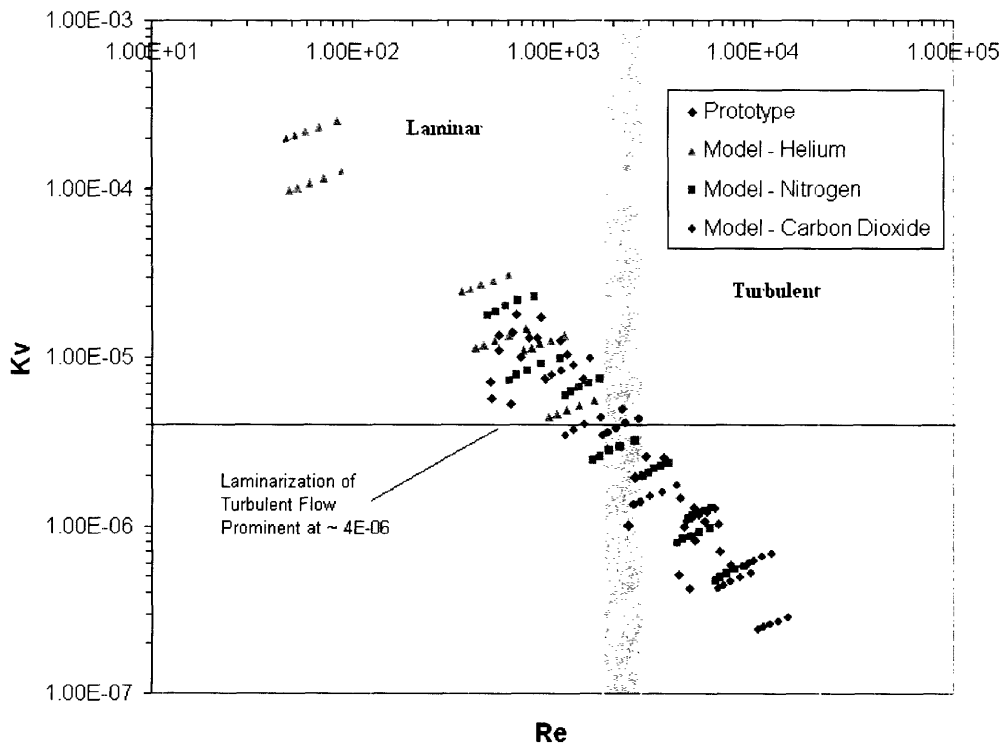
Figure 3-17 Range of acceleration parameter generated from experimental loop

References

1. Burmeister, L. C., Convective Heat Transfer, 2nd Edition, Chapter 10 , John Wiley & Sons, Inc., 1993.

2. Jackson, J. D., Cotton, M. A., and Axcell, B. P., "Studies of mixed convection in vertical tubes," *International Journal of Heat and Fluid Flow*, Vol. 10, No. 1, pp. 2-15, 1989.

3. McEligot D.M. and Jackson J.D., "Deterioration Criteria for Convective Heat Transfer in Gas Flow Through Non Circular Ducts," INEEL/JOU-03-01311, INEEL Report, Revised 2004. Also published in *Nuclear Engineering and Design*, 2004.

4. Williams W. C., Hejzlar P., Driscoll M. J., Lee W. J., and Saha P., "Analysis of a Convection Loop for GFR Post-LOCA Decay-Heat Removal from a Block- Type Core," Topical Report MIT-ANP-TR-095, Massachusetts Institute of Technology, Department of Nuclear Engineering, 2003.

4. LOOP CONSTRUCTION

Having verified that the proposed experimental loop design can operate in the flow regimes of interest, the next stage in the project was construction of the loop. Actual fabrication of the experimental loop was broken down into three stages. In the first stage the components of the loop, as described in Table 3-1, along with the power supply and forced convection system are assembled. In the second stage the instrumentation necessary for acquiring experimental data for use in calculating heat transfer coefficients and non-dimensional parameters is installed in the loop. Finally in the last stage insulation and guard heaters are applied to the test section and hot leg of the loop to reduce heat loss to the environment and maintain bulk fluid temperature.

4.1 Main Components

The entire loop is composed of Stainless Steel 316 tubing with an inner diameter of 25.4 mm, with the exception of the test section, which either has an inner diameter of 16 or 32 mm. The various sections of the loop are connected with stainless steel compression fittings. The test section is connected to the rest of the loop by reducing unions. Furthermore this transition has been made as smooth as possible as a taper has been inserted just upstream of the test section to ensure minimum disturbance while the fluid flow is developing.

A counter flow tube in tube heat exchanger was selected for the loop as it best met the heat transfer requirements of the loop. The heat exchanger itself is composed of 6 loops with an average diameter of 30.5cm (12 in) for an overall length of approximately 5.75m. However the heat exchanger from the top to bottom coil is only roughly 0.5m, half the height of the heat exchanger used in the LOCA-COLA analysis, which as a result actually provides a slight increase in the available driving head for natural circulation. Furthermore since the heat exchanger length assumed in the LOCA-COLA analysis was 2m the actual length of 5.75m will be more than sufficient to cool bulk fluid temperatures below 100°C. Also over-cooling of the fluid will not be an issue since the flow rate of the cooling water into the heat exchanger can be adjusted.

The test section will be resistively heated utilizing a 1500-ampere DC power supply. The power supply is connected to the exterior wall of the test section by a copper clamp at the bottom of the test section and by a stainless steel bar, welded directly to the tubing, at the top of the test

section. The level of heat input to the test section will be correlated with the electrical current provided by the power supply.

While the majority of the experimental trials will be conducted utilizing natural circulation, forced convection regimes can only be reached in the experiment with the addition of an external driving force. A forced convection system consisting of a compressor connected to an accumulator tank provides this driving force. Fluid flow is first branched off of the bottom horizontal section of the loop and taken to the compressor. The flow is then directed into the accumulator tank, where the compressed flow is smoothed before re-entering the main loop. From there the flow is reintroduced into the main loop through another valve located in the bottom section of the loop.

4.2 Instrumentation

In order to calculate heat transfer coefficients knowledge of the wall temperatures, heat deposited in the fluid, fluid velocities, and pressure drops in the system is required. As a result extensive instrumentation for the experimental loop is required. Figure 4-1 is a complete Process and Instrumentation Diagram for the experimental loop. The rest of this section is a detailed description of the instrumentation beginning with the test section and moving in the direction of the flow as depicted in Figure 4-1.
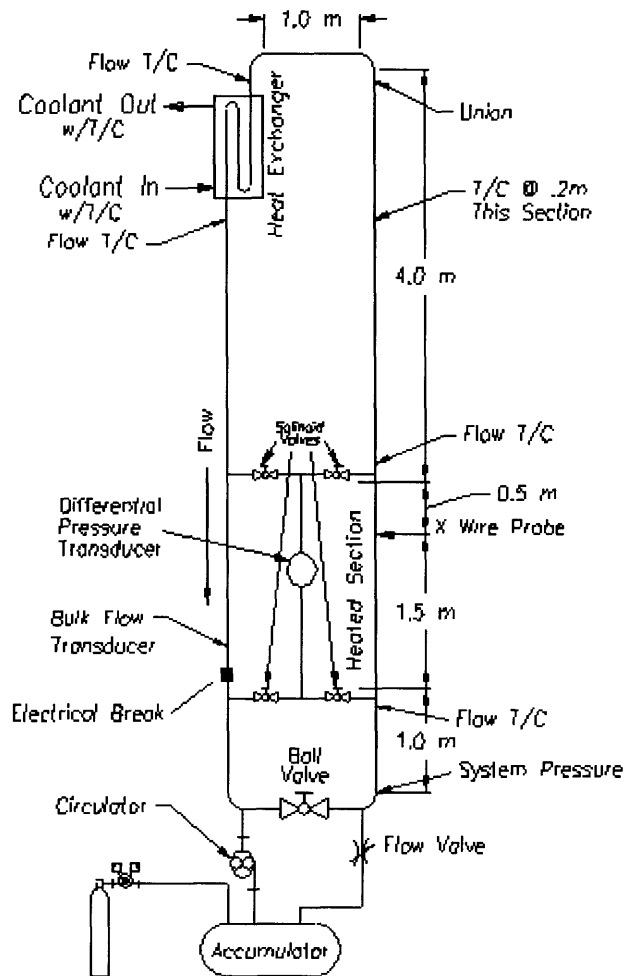
Figure 4-1 Process and instrumentation diagram

Type K wall thermocouples will be welded to the exterior of the test section every 10 cm to provide a basis for calculating the heat transfer coefficient of the gas. Shielded type K thermocouples will be placed in the bulk fluid just before and after the heated test section to measure the bulk fluid temperature. These bulk fluid temperature measurements will allow us to establish a correlation between the current applied to the test section and the heat deposited in the test section. An MKS Type 120 differential pressure transducer with a range of 1 Torr will be used to measure the pressure change across the heated test section. Measuring the pressure drop across the test section will serve two purposes. One, the measured experimental pressure drop can be compared to the pressure drop calculated from LOCA-COLA. And two, knowledge of the

46

pressure drop in conjunction with knowledge of the flow regime can be used to determine fluid velocity. A hot-wire probe will also be mounted in the test section in order to measure the local velocity and temperature profile of the fluid. After leaving the test section the fluid enters the vertical section of the hot leg of the loop where type K thermocouples are welded to the exterior of the tubing at the bottom, middle, and top of the section. The temperature readings from these thermocouples are used to ensure that the fluid is retaining heat for natural circulation purposes. From the hot leg of the loop the fluid enters the heat exchanger, where shielded type K thermocouples are placed in the bulk fluid at the inlet and outlet of the heat exchanger. These thermocouples will be used to calculate the heat removed from the fluid and to ensure that the temperature of the bulk fluid at the exit of the heat exchanger does not exceed 100°C. After leaving the heat exchanger the fluid enters the cold leg of the loop. The pressure drop in the vertical section of the cold leg of the loop is measured with the same MKS Type 120 differential pressure transducer used to measure the pressure drop in the test section. This will be accomplished through the use of solenoid valves that will allow the pressure transducer to switch between the test section and the cold leg. A bulk flow transducer will also be installed in the cold leg to measure the fluid velocity.

4.3 Insulation and Guard Heaters

One of the primary design concerns for the experimental loop is the issue of heat loss from the fluid to the environment, in both the heated test section and the hot leg of the loop. For the heated test section, heat loss is important as it directly impacts how much heat is added to the fluid, which is necessary for the calculation of the heat transfer coefficient. Heat loss is important in the hot leg as the temperature difference between the hot leg and the cold leg provides the driving force for natural circulation. Furthermore since we would like to run as many cases as possible under natural circulation we would like to minimize the heat loss to insure a maximum driving force. To this end both the test section and hot leg of the loop were insulated with two 2-inch thick layers of mineral wool pipe insulation with the following thermal conductivity profile:

47

Table 4-1 Insulation thermal conductivity

Mean Temperature °C	Thermal Conductivity W/m-°C
38	0.036
93	0.042
149	0.051
204	0.059
260	0.070
316	0.081
371	0.093

The purpose of the following section is to determine if the insulation provides adequate reduction in heat loss to the environment for both the test section and hot leg of the loop.

4.3.1 Test Section Heat Loss Analysis

The purpose of the experimental loop is to determine heat transfer correlations for a mixed convection regime. In order to accomplish this objective we will need to calculate heat transfer coefficients of various flow regimes based upon experimental data. The heat transfer coefficient is given by the following equation:

$$h = \frac{q''_{net}}{(T_{wi} - T_{bulk})}$$ (4-1)

In the preceding equation, the net heat flux term, q''_{net}, can only be determined after the test section heat has been calculated. The heat loss in the test section can be obtained from the following equations:

$$\dot{Q} = \frac{T_{wo} - T_{air}}{\Sigma R}$$ (4-2)

$$\Sigma R = \frac{\ln(d_{in}/d_o)}{2\pi k_{in}L} + \frac{1}{h_{air}\pi d_{in}L}$$ (4-3)

d_{in} = Outer diameter of insulation
d_o = Outer diameter of tubing/Inner diameter of insulation
T_{wo} = Temperature of outer wall
T_{air} = Temperature of ambient air
k_{in} = Thermal conductivity of insulation
h_{air} = Heat transfer coefficient of air
L = Length of interest

The heat transfer coefficient for air in equation 4-3 can be calculated for free convection over a cylinder using the following equations: [Schmidt et al, 1993]

$$h_{air} = \frac{\overline{Nu}k}{L}$$ (4-4)

$$\overline{Nu} = \left[\overline{Nu_0}^{1/2} + \left(\frac{Ra * \xi Pr}{300} \right)^{1/6} \right]^2$$ (4-5)

$$\xi Pr = \left[1 + \left(\frac{0.5}{Pr} \right)^{9/16} \right]^{-16/9}$$ (4-6)

What is most noticeable about equation 4-2 is the fact that if we assume a constant ambient temperature of 20°C there is really only one variable, the wall temperature. All of the other terms stay the same regardless of the fluid or pressure conditions. As a result we can expect our test section heat losses to increase with increasing wall temperature. Utilizing the wall temperatures calculated from LOCA-COLA, heat losses for the various LOCA-COLA input cases outlined in Chapter 3 can be calculated.

Table 4.2 Test section heat losses

Fluid	Test Section I.D. (mm)	Pressure (MPa)	Mass FlowRate (kg/s)	Deposited Heat (W)	T_{wall} Max(°C)	Heat Loss(W)	% Heat Deposited Lost
He	16	0.2	2.25E-5	50	457	66	132.0
He	16	0.6	1.87E-4	402	489	85	21.1
He	16	1.0	4.25E-4	804	512	108	13.4
N_2	16	0.1	2.54E-4	111	521	104	93.7
N_2	16	0.2	6.62E-4	251	611	170	67.7
N_2	16	0.6	1.73E-3	553	565	134	24.2
N_2	16	1.0	2.69E-3	804	557	139	17.3
CO_2	16	0.1	4.88E-4	211	623	178	84.4
CO_2	16	0.2	1.00E-3	327	632	154	47.1
CO_2	16	0.6	2.60E-3	704	517	127	18.0
CO_2	16	1.0	4.14E-3	1005	511	130	12.9

*Heat loss values are for fixed outer wall temperature profile, which was calculated using LOCA-COLA under the assumption of adiabatic outer wall boundary condition.

From Table 4.2 it is apparent that there will be significant heat losses in the test section. And since LOCA-COLA assumes heat is deposited in the fluid under adiabatic outer wall conditions, we will have to modify the heat input from theoretical input to experimental input. The amount of current we output from our DC power supply will have to account for both heat loss to the environment and heat deposited in the fluid. However such a process is complicated considering that for many cases the heat loss to the environment will be greater than the amount of heat deposited in the test fluid. As a result in addition to insulating the loop further steps must be taken to reduce heat loss to the environment. The most effective way to reduce the heat loss is to employ guard heaters to lessen the temperature gradient from the fluid to the outside temperature of the insulation. From equation 4-2 we know that the heat loss is linearly proportional to the temperature difference between the exterior wall temperature of the test section and the surface temperature of the insulation. A guard heater will be placed in between the two layers of insulation. Control thermocouples placed just under the outer surface of the inner layer will

50

match the temperature of the inner layer of insulation to the wall temperature of the test section. However, applying guard heaters in this case is not a trivial matter as the wall temperature varies with height along the test section. In order to account for the temperature variation three separate zones of PID control will be used for matching the insulation temperature to the wall temperature.

4.3.2 Hot Leg Heat Loss Analysis

For the purposes of heat loss calculation the hot leg of the loop will be divided into ten 0.5 m sections. For each section the heat loss will be calculated along with the corresponding decrease in bulk fluid temperature. For the first section, the bulk fluid temperature is simply the outlet temperature of the heated test section. The heat loss from the fluid to the outside environment can be determined by the following equation:

$$\dot{Q} = \frac{T_B - T_{air}}{\Sigma R} \tag{4-7}$$

The heat loss depends upon three factors; the ambient air temperature, T_{air} (which we have previously assumed to be a constant 20°C), the thermal resistance between the fluid and outside environment, ΣR, and the bulk fluid temperature, T_B. The thermal resistance between the fluid and the outside environment can be calculated from the following equation:

$$\Sigma R = \frac{1}{h_{gas} \pi d_i L} + \frac{\ln(d_o / d_i)}{2 \pi k_{ss} L} + \frac{\ln(d_{in} / d_o)}{2 \pi k_{in} L} + \frac{1}{h_{air} \pi d_{in} L} \tag{4-8}$$

h_{gas} = Heat transfer coefficient of test fluid
k_{ss} = Thermal conductivity of stainless steel 316
d_i = Inner diameter of tubing

In the preceding equation the heat transfer coefficient for air was calculated in the manner outlined in section 4.3.1. Finally, the calculation of the bulk fluid temperature is a bit more involved, as a control volume analysis will be implemented for each section to calculate the bulk fluid temperature. All fluids were assumed to be ideal gases. Starting from the energy equation:

51

$$\frac{Q}{m} - \frac{W}{m} = c_p(T_{out} - T_{in}) + (V_{out}^2 - V_{in}^2)/2 + g\Delta z/2 \qquad (4\text{-}9)$$

We can readily eliminate three terms from the previous equation. First we can eliminate the work term as the fluid does no work in the control volume. Next we can eliminate both the velocity and gravity terms as they are negligible when compared to the temperature term. As a result we are left with the following equation for the bulk fluid temperature

$$T_{bulk} = T_{out} = T_{in} - \left(\frac{Q/m}{c_p}\right) \qquad (4\text{-}10)$$

Utilizing equations 4-7, 4-8, 4-10, we are able to calculate the bulk temperature of the fluid for each section of the hot leg and the resulting heat loss. The hot leg heat losses for the three fluids, helium, nitrogen, and carbon dioxide at various pressures are listed in Table 4-3 along with relevant system parameters.

Table 4-3 Hot leg heat losses

Fluid	Test Section I.D. (mm)	Pressure (MPa)	Mass FlowRate (kg/s)	Deposited Heat (W)	Heat Loss(W)	T_{bulk} Inlet(°C)	T_{bulk} Outlet(°C)
He	16	0.2	2.25E-5	50	51	456	20
He	16	0.6	1.87E-4	402	312	443	137
He	16	1.0	4.25E-4	804	391	411	247
N_2	16	0.1	2.54E-4	111	116	446	22
N_2	16	0.2	6.62E-4	251	251	435	97
N_2	16	0.6	1.73E-3	553	374	428	242
N_2	16	1.0	2.69E-3	804	421	435	302
CO_2	16	0.1	4.88E-4	211	232	485	68
CO_2	16	0.2	1.00E-3	327	303	419	161
CO_2	16	0.6	2.60E-3	704	392	409	284
CO_2	16	1.0	4.14E-3	1005	416	406	323

Table 4.3 illustrates just how damaging heat loss in the hot leg can be as in many cases there is a significant decrease in the bulk temperature of the fluid. Specifically we see quite a large decrease in bulk fluid temperature for cases with low mass flow rates, on the order of 10^{-4}-10^{-5}, and low deposited heat, on the order of a couple hundred watts or less. For the aforementioned cases, natural circulation is severely limited as the density difference between the hot and cold legs of the loop significantly decreases. However, it should also be noted, that the effect of the heat loss on the bulk fluid temperature is somewhat mitigated by depositing more heat in the test section, as is demonstrated by the carbon dioxide example, where the bulk fluid temperature decreases from 406 °C to 323 °C. But the majority of our experimental runs, especially those designed to operate in a laminar regime, will have relatively low deposited heats and resulting large drops in bulk fluid temperature. As a result, we must significantly reduce the heat loss in the hot leg of the loop. Guard heaters will once again be employed as described in the previous section to reduce the temperature gradient between the inner layer of insulation and the outer wall of the tubing.

References

1. Schmidt, F.W., Henderson, R.E., Wolgemuth, C.H., Introduction to Thermal Sciences, 2nd ed., John Wiley & Sons, p. 248-252, 1993.

5. EXPERIMENTAL LOOP UNCERTAINTY ANALYSIS

The experimental loop and its attendant instrumentation discussed in the previous two chapters is designed to collect experimental data in a variety of flow regimes for use in the formulation of heat transfer correlations. However up to this point we have only proved that the experimental loop will be capable of obtaining the desired data in the desired flow regimes. The accuracy of the data must be verified before it is put to use in the formulation of heat transfer correlations. As mentioned in the previous chapter, the primary data collected from the loop will be used to calculate the heat transfer coefficient, h, and the important non-dimensional parameters. The following uncertainty analysis is limited to the heat transfer coefficient as it would be premature to calculate the uncertainty for non-dimensional parameters as we have no set form for a heat transfer correlation.

5.1 Theoretical Uncertainty Analysis

For the purposes of uncertainty analysis, the test section has been divided into n nodes each having length L_{node}. The following derivation of the relative uncertainty in the heat transfer coefficient is based upon the heat transfer analysis of one of these nodes. The experimental heat transfer coefficient for the node (Figure 5-1) is obtained from the following equation:

$$h = \frac{q''_{net}}{(T_{wi} - T_{bulk})} \tag{5-1}$$
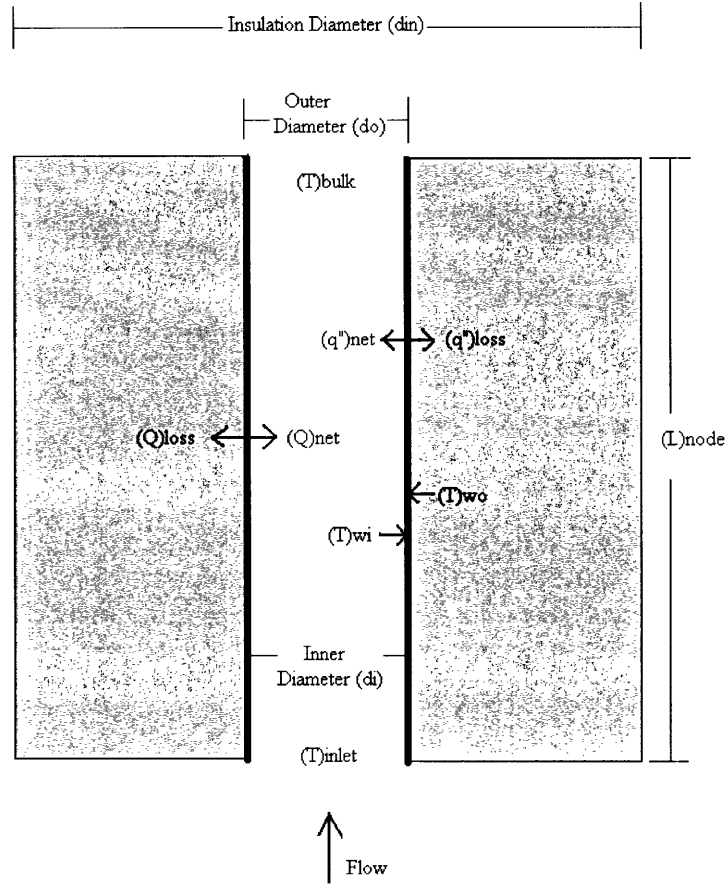
Figure 5-1 Sample Node from Test Section

For the purposes of our uncertainty analysis we will use the following equation from Kline and McClintock [1953] to determine the uncertainty in the calculated heat transfer coefficient:

$$\Delta R = \left[\left(\frac{\partial R}{\partial v_1} \Delta v_1 \right)^2 + \left(\frac{\partial R}{\partial v_2} \Delta v_2 \right)^2 \ldots + \left(\frac{\partial R}{\partial v_n} \Delta v_3 \right)^2 \right]^{1/2}$$

(5-2)

$R = Linear\ Function\ of\ n\ \mathrm{variables} = R(v_1, v_2, \ldots v_n)$

When this equation is applied to equation 5-1 we are left with the following expression for the uncertainty in the heat transfer coefficient calculation:

$$\Delta h = \left[\left(\frac{\Delta q''_{net}}{T_{wi} - T_{bulk}} \right)^2 + \left(\frac{q''_{net} \Delta T_{wall}}{(T_{wi} - T_{bulk})^2} \right)^2 + \left(\frac{q''_{net} \Delta T_{bulk}}{(T_{wi} - T_{bulk})^2} \right)^2 \right]^{\frac{1}{2}}$$

(5-3)

55

This equation can further be simplified by dividing both sides by the heat transfer coefficient to create a non-dimensional form:

$$\frac{\Delta h}{h} = \left[\left(\frac{\Delta q''_{net}}{q''_{net}} \right)^2 + \left(\frac{\Delta T_{wi}}{(T_{wi} - T_{bulk})} \right)^2 + \left(\frac{\Delta T_{bulk}}{(T_{wi} - T_{bulk})} \right)^2 \right]^{\frac{1}{2}}$$

(5-4)

In order to arrive at a numerical answer for the relative uncertainty in the heat transfer coefficient calculation we must first determine the heat flux, bulk fluid temperature, and wall temperature absolute uncertainty terms.

5.1.1 Net Heat Flux Uncertainty Term

The net heat flux is given by the following equation:

$$q''_{net} = \frac{d_o}{d_i} (q''_{total} - q''_{loss})$$

(5-5)

The do/d$_i$ term is a correction factor that arises from the fact that the total heat flux and the heat flux loss terms are calculated at the outside of the test section tube while the net heat flux term must be calculated at the inside of the test section tube for heat transfer coefficient analysis. Application of equation 5-2 yields the following expression for the uncertainty in the net heat flux term:

$$\Delta q''_{net} = \left[\begin{array}{l} \left(\frac{(q''_{total} - q''_{loss}) \Delta d_o}{d_i} \right)^2 + \left(\frac{d_o (q''_{total} - q''_{loss}) \Delta d_i}{d_i^2} \right)^2 \\ + \left(\frac{d_o \Delta q''_{total}}{d_i} \right)^2 + \left(\frac{d_o \Delta q''_{loss}}{d_i} \right)^2 \end{array} \right]^{\frac{1}{2}}$$

(5-6)

Of the four uncertainty terms in the previous equation, Δd_o and Δd_i are known as they are manufacturing tolerances of the test section tube. The uncertainty terms for total heat flux and heat flux loss must be calculated. First the total heat flux, due to resistive heating, can be calculated from the following equation:

$$q_{total}^{''} = \frac{I^2 R_{node}}{\pi d_o L_{node}}$$
(5-7)

In the preceding equation R is the electrical resistance offered by the test section node and is given by the following equation:

$$R_{node} = \frac{\rho L_{node}}{A} = \frac{4\rho L_{node}}{\pi (d_o^2 - d_i^2)}$$
$$\rho = resistivity \ (\Omega - m)$$
(5-8)

Substituting our expression for the resistance back into equation 5-7 yields the following expression for the total heat flux:

$$q_{total}^{''} = \frac{4I^2 \rho}{\pi^2 (d_o^3 - d_o d_i^2)}$$
(5-9)

Once again we can apply equation 5-2 to determine the absolute uncertainty:

$$\Delta q_{total}^{''} = \left[\left(\frac{8I\rho\Delta I}{\pi^2 (d_o^3 - d_o d_i^2)} \right)^2 + \left(\frac{4I^2 \Delta\rho}{\pi^2 (d_o^3 - d_o d_i^2)} \right)^2 + \left(\frac{4I^2 \rho (3d_o^2 - d_i^2)\Delta d_o}{\pi^2 (d_o^3 - d_o d_i^2)^2} \right)^2 + \left(\frac{8I^2 \rho d_i d_o \Delta d_i}{\pi^2 (d_o^3 - d_o d_i^2)^2} \right)^2 \right]^{\frac{1}{2}}$$
(5-10)

All four of the uncertainty terms in the equation are known, and as a result we need go no further in the uncertainty analysis of the total heat flux. Next, the heat flux loss can be calculated from the following equation:

$$q_{loss}^{"} = \frac{T_{wo} - T_{air}}{\Sigma R_{thermal}} = \frac{T_{wo} - T_{air}}{\dfrac{d_o \ln(d_{in}/d_o)}{2k_{in}} + \dfrac{d_o}{h_{air}d_{in}}}$$

$k_{in} = thermal\ conductivity\ insulation\ (W/m\cdot C)$

$h_{air} = heat\ transfer\ coefficient\ air\ (W/m^2\cdot C)$

(5-11)

After applying equation 5-2 we are left with the following equation for the uncertainty in the heat flux loss term:

$$\Delta q_{loss}^{"} = \left[\left(\frac{\Delta T_{wo}}{\dfrac{d_o \ln(d_{in}/d_o)}{2k_{in}} + \dfrac{d_o}{h_{air}d_{in}}} \right)^2 + \left(\frac{\Delta T_{air}}{\dfrac{d_o \ln(d_{in}/d_o)}{2k_{in}} + \dfrac{d_o}{h_{air}d_{in}}} \right)^2 + \right.$$
$$\left(\frac{(T_{wo} - T_{air})(\dfrac{d_o}{2k_{in}d_{in}} - \dfrac{d_o}{h_{air}d_{in}^2})\Delta d_{in}}{(\dfrac{d_o \ln(d_{in}/d_o)}{2k_{in}} + \dfrac{d_o}{h_{air}d_{in}})^2} \right)^2 +$$
$$\left(\frac{(T_{wo} - T_{air})\left(\dfrac{\ln(d_{in}/d_o)}{2k_{in}} - \dfrac{1}{2k_{in}} + \dfrac{1}{h_{air}d_{in}} \right)\Delta d_o}{(\dfrac{d_o \ln(d_{in}/d_o)}{2k_{in}} + \dfrac{d_o}{h_{air}d_{in}})^2} \right)^2 +$$
$$\left. \left(\frac{(T_{wo} - T_{air})\left(\dfrac{d_o \ln(d_{in}/d_o)}{2k_{in}^2} \right)\Delta k_{in}}{(\dfrac{d_o \ln(d_{in}/d_o)}{2k_{in}} + \dfrac{d_o}{h_{air}d_{in}})^2} \right)^2 + \left(\frac{(T_{wo} - T_{air})\left(\dfrac{d_o}{h_{air}^2 d_{in}} \right)\Delta h_{air}}{(\dfrac{d_o \ln(d_{in}/d_o)}{2k_{in}} + \dfrac{d_o}{h_{air}d_{in}})^2} \right)^2 \right]^{\frac{1}{2}}$$

(5-12)

58

Although this equation is quite lengthy every single uncertainty term is known, as a result the expressions for the total heat flux and heat flux loss uncertainty terms can be plugged back into the net heat flux uncertainty equation (equation 5-6) to yield a value for the uncertainty associated with the net heat flux.

5.1.2 Bulk Fluid Temperature Uncertainty Term

The bulk fluid temperature is given by the following equation:

$$T_{bulk} = T_i + \frac{(Q_{total} - Q_{loss})}{\dot{m} c_p}$$

(5-13)

It should be noted that the initial temperature for the first node is the temperature measured by the flow thermocouple at the inlet of the test section while for every node after that the inlet temperature is simply the bulk fluid temperature of the previous node. This is an important distinction as it means the uncertainty in the bulk fluid temperature will be compounded as one progresses up the heated test section. Once again we will apply equation 5-2 to determine the uncertainty in the bulk fluid temperature:

$$\Delta T_{bulk} = \left[\begin{array}{l} (\Delta T_i)^2 + \left(\dfrac{\Delta Q_{total}}{\dot{m} c_p}\right)^2 + \left(\dfrac{\Delta Q_{loss}}{\dot{m} c_p}\right)^2 + \\[4mm] \left(\dfrac{(Q_{total} - Q_{loss})\Delta \dot{m}}{\dot{m}^2 c_p}\right)^2 + \left(\dfrac{(Q_{total} - Q_{loss})\Delta c_p}{\dot{m} c_p^2}\right)^2 \end{array} \right]^{\frac{1}{2}}$$

(5-14)

Of the uncertainty terms in the previous equation only the inlet temperature and the constant pressure specific heat uncertainties are known, the rest must be derived. The total heat can be calculated from the following equation:

$$Q_{total} = I^2 R_{node} = \frac{4I^2 \rho L_{node}}{\pi(d_o{}^2 - d_i{}^2)}$$ (5-15)

Application of equation 5-2 yields the following final equation for the uncertainty in the total heat:

$$\Delta Q_{total} = \begin{bmatrix} \left(\dfrac{8I\rho L_{node}\Delta I}{\pi(d_o{}^2 - d_i{}^2)} \right)^2 + \left(\dfrac{4I^2 L_{node}\Delta\rho}{\pi(d_o{}^2 - d_i{}^2)} \right)^2 + \left(\dfrac{4I^2 \rho\Delta L_{node}}{\pi(d_o{}^2 - d_i{}^2)} \right)^2 + \\ \left(\dfrac{8I^2 \rho L_{node}d_o\Delta d_o}{\pi(d_o{}^2 - d_i{}^2)^2} \right)^2 + \left(\dfrac{8I^2 \rho L_{node}d_i\Delta d_i}{\pi(d_o{}^2 - d_i{}^2)^2} \right)^2 \end{bmatrix}^{\frac{1}{2}}$$ (5-16)

Next, the heat loss term can be calculated from the following equation:

$$Q_{loss} = \frac{T_{wo} - T_{air}}{\dfrac{\ln(d_{in}/d_o)}{2\pi k_{in} L_{node}} + \dfrac{1}{\pi d_{in} L_{node} h_{air}}}$$ (5-17)

The corresponding uncertainty term is as follows:

$$\Delta Q_{loss} = \left[\left(\frac{\Delta T_{wo}}{\frac{\ln(d_{in}/d_o)}{2\pi k_{in} L_{node}} + \frac{1}{\pi d_{in} L_{node} h_{air}}} \right)^2 + \left(\frac{\Delta T_{air}}{\frac{\ln(d_{in}/d_o)}{2\pi k_{in} L_{node}} + \frac{1}{\pi d_{in} L_{node} h_{air}}} \right)^2 + \right.$$

$$\left(\frac{(T_{wo} - T_{air})\left(\frac{1}{2\pi k_{in} L_{node} d_{in}} - \frac{1}{\pi L_{node} h_{air} d_{in}^2} \right) \Delta d_{in}}{\left(\frac{\ln(d_{in}/d_o)}{2\pi k_{in} L_{node}} + \frac{1}{\pi d_{in} L_{node} h_{air}} \right)^2} \right)^2 +$$

$$\left(\frac{(T_{wo} - T_{air})\left(\frac{1}{2\pi k_{in} L_{node} d_o} \right) \Delta d_o}{\left(\frac{\ln(d_{in}/d_o)}{2\pi k_{in} L_{node}} + \frac{1}{\pi d_{in} L_{node} h_{air}} \right)^2} \right)^2 + \left(\frac{(T_{wo} - T_{air})\left(\frac{\ln(d_{in}/d_o)}{2\pi L_{node} k_{in}^2} \right) \Delta k_{in}}{\left(\frac{\ln(d_{in}/d_o)}{2\pi k_{in} L_{node}} + \frac{1}{\pi d_{in} L_{node} h_{air}} \right)^2} \right)^2 + \tag{5-18}$$

$$\left(\frac{(T_{wo} - T_{air})\left(\frac{\ln(d_{in}/d_o)}{2\pi k_{in} L_{node}^2} + \frac{1}{\pi d_{in} L_{node}^2 h_{air}} \right) \Delta L_{node}}{\left(\frac{\ln(d_{in}/d_o)}{2\pi k_{in} L_{node}} + \frac{1}{\pi d_{in} L_{node} h_{air}} \right)^2} \right)^2 +$$

$$\left. \left(\frac{(T_{wo} - T_{air})\left(\frac{1}{\pi d_{in} L_{node} h_{air}^2} \right) \Delta h_{air}}{\left(\frac{\ln(d_{in}/d_o)}{2\pi k_{in} L_{node}} + \frac{1}{\pi d_{in} L_{node} h_{air}} \right)^2} \right)^2 \right]^{\frac{1}{2}}$$

The last uncertainty term to be derived for the bulk fluid temperature is for the mass flow rate. In the experiment we will use a sensitive differential pressure transducer to measure a pressure drop across a specific length in the cold leg of the loop. We will then equate this pressure drop to the head loss due to friction by the following equation:

$$\Delta p = \frac{\rho f L V^2}{2 d_H} \tag{5-19}$$

However equation 5-19 is not as simple as it seems as the friction factor, f, depends upon the Re number.

$$f = \frac{64}{\text{Re}} \quad (\text{Re} < 2000) \tag{5-20}$$

$$f = \frac{0.3164}{\text{Re}^{1/4}} \quad (\text{Re} > 4000) \tag{5-21}$$

Furthermore, as we have two different equations for the friction factor, based upon Re number, we will need to develop two expressions for the mass flow rate, one for laminar flow and one for turbulent flow. For laminar flow (Re<2000) the mass flow rate is defined as follows:

$$\dot{m}_{lam} = \frac{\pi \rho \Delta p d_h^4}{128 \mu L_{test}}$$

$\rho = $ fluid density

$\Delta p = $ measured pressure drop

$d_h = $ hydraulic diameter   (5-22)

$\mu = $ dynamic viscosity

$L_{test} = $ length of pressure drop measurement

The corresponding uncertainty term for the laminar mass flow rate is:

$$\Delta \dot{m}_{lam} = \left[\begin{array}{l} \left(\dfrac{\pi \Delta p d_h^4 \Delta \rho}{128 \mu L_{test}}\right)^2 + \left(\dfrac{\pi \rho d_h^4 \Delta(\Delta p)}{128 \mu L_{test}}\right)^2 + \left(\dfrac{\pi \rho \Delta p d_h^3 \Delta d_h}{32 \mu L_{test}}\right)^2 + \\[4mm] \left(\dfrac{\pi \rho \Delta p d_h^4 \Delta \mu}{128 \mu^2 L_{test}}\right)^2 + \left(\dfrac{\pi \rho \Delta p d_h^4 \Delta L_{test}}{128 \mu L_{test}^2}\right)^2 \end{array} \right]^{\frac{1}{2}} \tag{5-23}$$

The mass flow rate for turbulent flows (Re>4000) is defined by the following equation:

62

$$\dot{m}_{turb} = \frac{0.717\pi\rho^{4/7}\Delta p^{4/7}d_h^{19/7}}{\mu^{1/7}L_{test}^{4/7}} \tag{5-24}$$

And the corresponding uncertainty term for the turbulent mass flow rate is:

$$\Delta \dot{m}_{turb} = \left[\begin{array}{l} \left(\dfrac{0.410\pi\rho^{-3/7}\Delta p^{4/7}d_h^{19/7}\Delta\rho}{\mu^{1/7}L_{test}^{4/7}}\right)^2 + \left(\dfrac{0.410\pi\rho^{4/7}\Delta p^{-3/7}d_h^{19/7}\Delta(\Delta p)}{\mu^{1/7}L_{test}^{4/7}}\right)^2 \\[4mm] + \left(\dfrac{1.946\pi\rho^{4/7}\Delta p^{4/7}d_h^{12/7}\Delta d_h}{\mu^{1/7}L_{test}^{4/7}}\right)^2 + \left(\dfrac{0.102\pi\rho^{4/7}\Delta p^{4/7}d_h^{19/7}\Delta\mu}{\mu^{8/7}L_{test}^{4/7}}\right)^2 \\[4mm] + \left(\dfrac{0.410\pi\rho^{4/7}\Delta p^{4/7}d_h^{19/7}\Delta L_{test}}{\mu^{1/7}L_{test}^{11/7}}\right)^2 \end{array} \right]^{\frac{1}{2}} \tag{5-25}$$

It should also be noted at this point that we do not have an equation for the mass flow rate for a Reynolds number range of 2000-4000. However the experimental loop will also be used by another researcher to measure velocity profiles, and we can use the hot-wire probe required for these measurements to determine the mass flow rate for the Reynolds number range of 2000-4000. Having developed equations for the uncertainty associated with the total heat rate, heat loss, and mass flow rate, we can now generate a numerical answer for the uncertainty associated with the calculated bulk fluid temperature.

5.1.3 Wall Temperature Uncertainty Term

The inner wall temperature is given by the following equation:

$$T_{wi} = T_{wo} - (Q_{total} - Q_{loss})R_{thermal} \tag{5-26}$$

Substituting the expression for the thermal resistance into equation 5-26 we are left with the following expression for the inner wall temperature:

$$T_{wi} = T_{wo} - (Q_{total} - Q_{loss})\frac{\ln(d_o / d_i)}{2\pi k_{ss} L_{node}}$$

(5-27)

The uncertainty associated with the inner wall temperature can then be determined by the application of equation 5-2:

$$\Delta T_{wall} = \left[\begin{array}{l} (\Delta T_{wo})^2 + \left(\dfrac{\ln(d_o / d_i)\Delta Q_{total}}{2\pi k_{ss} L_{node}}\right)^2 + \left(\dfrac{\ln(d_o / d_i)\Delta Q_{loss}}{2\pi k_{ss} L_{node}}\right)^2 + \\[3ex] \left(\dfrac{(Q_{total} - Q_{loss})\ln(d_o / d_i)\Delta k_{ss}}{2\pi k_{ss}{}^2 L_{node}}\right)^2 + \left(\dfrac{(Q_{total} - Q_{loss})\ln(d_o / d_i)\Delta L_{node}}{2\pi k_{ss} L_{node}{}^2}\right)^2 \\[3ex] + \left(\dfrac{(Q_{total} - Q_{loss})\Delta d_o}{2\pi k_{ss} L_{node} d_o}\right)^2 + \left(\dfrac{(Q_{total} - Q_{loss})\Delta d_i}{2\pi k_{ss} L_{node} d_i}\right)^2 \end{array} \right]^{\frac{1}{2}}$$

(5-28)

5.1.4 Theoretical Uncertainty Analysis Summary

In order to calculate the relative uncertainty of our experimental heat transfer coefficients the total uncertainty in the heat transfer coefficient calculation was broken down into three terms, net heat flux uncertainty, wall temperature uncertainty, and bulk fluid temperature uncertainty. Each of these three terms was in turn further broken down until all three of the terms contained only numerically defined uncertainty terms.

5.2 Initial Numerical Uncertainty Analysis

First, in order to calculate the relative uncertainty for the heat transfer coefficient; we need to know input parameters and their absolute uncertainties. In some cases we know the absolute uncertainties associated with the parameters, while in others we must calculate the absolute uncertainty based upon the value of the parameter in question and its associated relative uncertainty. Table 5.1 is a list of both absolute and relative uncertainties for all fluid-independent quantities associated with the uncertainty analysis of the heat transfer coefficient.

Table 5.1 Absolute and relative uncertainties for fluid-independent parameters

Parameter	Value	Absolute Uncertainty	Relative Uncertainty	Source
d_i	0.01575 m	0.0001 m	0.63 %	Estimate
d_o	0.01905 m	0.0001 m	0.52 %	Estimate
d_{in}	0.22225 m	0.001 m	0.45 %	Estimate
d_h	0.0254 m	0.0001 m	0.39 %	Estimate
I	Variable (A)	1.0 A	Variable	Estimate
h_{air}	5 W/m^2-°C	1 W/m^2-°C	20 %	Estimate
P	Variable (Ω-m)	Variable	5 %	Estimate
k_{in}	Variable (W/m-°C)	Variable	5 %	Estimate
k_{ss}	Variable (W/m-°C)	Variable	5 %	Estimate
L_{node}	0.05 m	0.001	2 %	Estimate
Δp	Variable (Pa)	Variable	0.25%	Manufacturer
L_{test}	6.75 m	0.001	0.015 %	Estimate
T_{air}	20 °C	0.5 °C	2.5 %	Manufacturer
c_p	Variable (J/kg-°C)	Variable	1.0 %	Literature

The fluid-dependent sources of uncertainty for the heat transfer coefficient were obtained from the NIST database [NIST 2000] and are listed in Table 5.2.

Table 5.2 Relative uncertainties for fluid-dependent parameters

Fluid	Relative Uncertainty μ (kg/m-s)	Relative Uncertainty ρ (kg/m^3)
He	10.0 %	0.10 %
N_2	2.0 %	0.02 %
CO_2	0.3 %	0.03 %

Having determined all of the uncertainty terms for the necessary parameters, we can now obtain relative uncertainties for the heat transfer coefficient for the calculated fluid trials of Chapter 3. Table 5.3 lists the ranges of the relative uncertainty in the heat transfer coefficient along with their corresponding Re and Ra number ranges.

Table 5.3 Heat transfer coefficient relative uncertainties

Fluid	ID (mm)	Pressure (MPa)	Flow Rate (kg/s)	Deposited Heat (W)	Re Range	Ra Range	$\Delta h/h$ Range
He	16	0.2	2.25E-5	50	89-49	1.02E3-1.32E1	0.51-15.29
He	16	0.6	1.87E-4	402	734-410	5.19E4-9.54E2	0.093-0.232
He	16	1.0	4.25E-4	804	1608-963	1.72E5-6.01E3	0.091-0.130
N2	16	0.1	2.54E-4	111	1088-607	1.11E5-2.42E3	0.112-0.613
N2	16	0.2	6.62E-4	251	2579-1595	4.20E5-1.94E4	0.114-0.206
N2	16	0.6	1.73E-3	553	6115-4200	5.98E6-4.31E5	0.096-0.126
N2	16	1.0	2.69E-3	804	9052-6473	1.76E7-1.69E6	0.093-0.113
CO2	16	0.1	4.88E-4	211	2247-1159	1.83E5-7.53E3	0.145-0.251
CO2	16	0.2	1.00E-3	327	4233-2549	1.50E6-6.27E4	0.102-0.180
CO2	16	0.6	2.60E-3	704	9868-6688	1.81E7-1.67E6	0.094-0.114
CO2	16	1.0	4.14E-3	1005	14914-10681	5.47E7-6.83E6	0.092-0.105

*Re, Ra, and $\Delta h/h$ ranges go from test section inlet to outlet

Before any conclusions can be drawn from Table 5.3, the $\Delta h/h$ range of 0.51-15.29 for the first helium case should be examined. There are two reasons why the relative uncertainty in the heat transfer coefficient is so large in this case. First we know from Table 4.3 that the test section heat loss is greater than the heat deposited in the test section and as a result the net heat flux goes to zero approximately 7/8 of the way up the test section and then to negative numbers at the outlet of the test section. This causes the first uncertainty term in equation 5-4 to blow up and drastically increase the overall uncertainty. The second reason for the large uncertainty is the fact that (T_{wall}-T_{bulk}) is on the order of 1 to 2 °C at the outlet of the test section, while the absolute

uncertainty in the bulk fluid temperature is on the order of 15 °C. This in turn causes the third uncertainty term in equation 5-4 to become quite large, generating a significant contribution to the overall uncertainty in the heat transfer coefficient. It is apparent from Table 5.3 that the relative uncertainty ranges are unacceptable for the majority of the calculated trials, especially for the trials designed to operate in the laminar regime. As a result, we must look for ways of reducing the uncertainty, either through more efficient calculations or improvements in the experimental loop design.

5.3 Uncertainty Reduction in Heat Transfer Coefficient Calculation

As was mentioned previously, the relative uncertainty associated with the heat transfer coefficient is given by the following equation:

$$\frac{\Delta h}{h} = \left[\left(\frac{\Delta q_{net}^{''}}{q_{net}^{''}} \right)^2 + \left(\frac{\Delta T_{wi}}{(T_{wi} - T_{bulk})} \right)^2 + \left(\frac{\Delta T_{bulk}}{(T_{wi} - T_{bulk})} \right)^2 \right]^{\frac{1}{2}} \tag{5-29}$$

Equation 5-29 is comprised of three terms, the uncertainty in the inner wall temperature, bulk fluid temperature, and net heat flux. As a result we have three different avenues of approach when trying to reduce the overall uncertainty in the heat transfer coefficient.

5.3.1 Inner Wall Temperature

From equation 5-29 it is apparent that there are two ways to decrease the ΔT_{wi} component of the heat transfer coefficient uncertainty, by either decreasing ΔT_{wi} or increasing $(T_{wi} - T_{bulk})$. However since $(T_{wi} - T_{bulk})$ is a product of fluid properties, mass flow rate, and heat deposited, we cannot increase $(T_{wi} - T_{bulk})$ without significantly changing the range of dimensionless parameters covered. As a result any effort to decrease the uncertainty in the inner wall temperature

component must focus solely on decreasing ΔT_{wi}. The uncertainty associated with the inner wall temperature is calculated from the following equation:

$$\Delta T_{wi} = \left[\begin{array}{l} (\Delta T_{wo})^2 + \left(\dfrac{\ln(d_o/d_i)\Delta Q_{total}}{2\pi k_{ss} L_{node}} \right)^2 + \left(\dfrac{\ln(d_o/d_i)\Delta Q_{loss}}{2\pi k_{ss} L_{node}} \right)^2 + \\[3mm] \left(\dfrac{(Q_{total}-Q_{loss})\ln(d_o/d_i)\Delta k_{ss}}{2\pi k_{ss}^{\ 2} L_{node}} \right)^2 + \left(\dfrac{(Q_{total}-Q_{loss})\ln(d_o/d_i)\Delta L_{node}}{2\pi k_{ss} L_{node}^{\ 2}} \right)^2 \\[3mm] + \left(\dfrac{(Q_{total}-Q_{loss})\Delta d_o}{2\pi k_{ss} L_{node} d_o} \right)^2 + \left(\dfrac{(Q_{total}-Q_{loss})\Delta d_i}{2\pi k_{ss} L_{node} d_i} \right)^2 \end{array} \right]^{\frac{1}{2}} \qquad (5\text{-}30)$$

From equation 5-30 it is apparent that there are quite a few sources of uncertainty in calculating the inner wall temperature. However of all the terms in equation 5-30 we can only manipulate the Q_{loss} term. Furthermore, looking at Table 5.4, we see that the Q_{loss} term will have little to no effect as the uncertainty in the inner wall temperature is due almost entirely to the uncertainty in the outer wall temperature (i.e., $\Delta T_{wi} \approx \Delta T_{wo}$ independently of the case). As a result, even if we were to minimize the uncertainty terms in equation 5-30 involving Q_{loss}, there would not be a noticeable decrease in the uncertainty associated with the inner wall temperature.

Table 5.4 Inner wall temperature uncertainty component

Fluid	Test Section I.D. (mm)	Pressure (MPa)	ΔT_{wo} (°C)	ΔT_{wi}* (°C)
He	16	0.2	1.0	1.000029
He	16	0.6	1.0	1.000420
He	16	1.0	1.0	1.001293
N_2	16	0.1	1.0	1.000074
N_2	16	0.2	1.0	1.000245
N_2	16	0.6	1.0	1.000699
N_2	16	1.0	1.0	1.001296
CO_2	16	0.1	1.0	1.000198
CO_2	16	0.2	1.0	1.000333
CO_2	16	0.6	1.0	1.001024
CO_2	16	1.0	1.0	1.001892

*maximum ΔT_{wi} for case

Also as part of our efforts to reduce uncertainty, we looked at replacing the existing wall thermocouples with more expensive, more accurate thermocouples, absolute uncertainty of ±0.1°C. However the more accurate thermocouples did not provide for a noticeable decrease in the overall uncertainty associated with the heat transfer coefficient. This can be attributed to the fact that the uncertainty in the inner wall temperature does not provide a significant contribution to the overall uncertainty in the heat transfer coefficient as illustrated in Figure 5-2. As a result we must look to the bulk fluid temperature and net heat flux for ways to reduce the overall uncertainty in the calculation of the heat transfer coefficient.
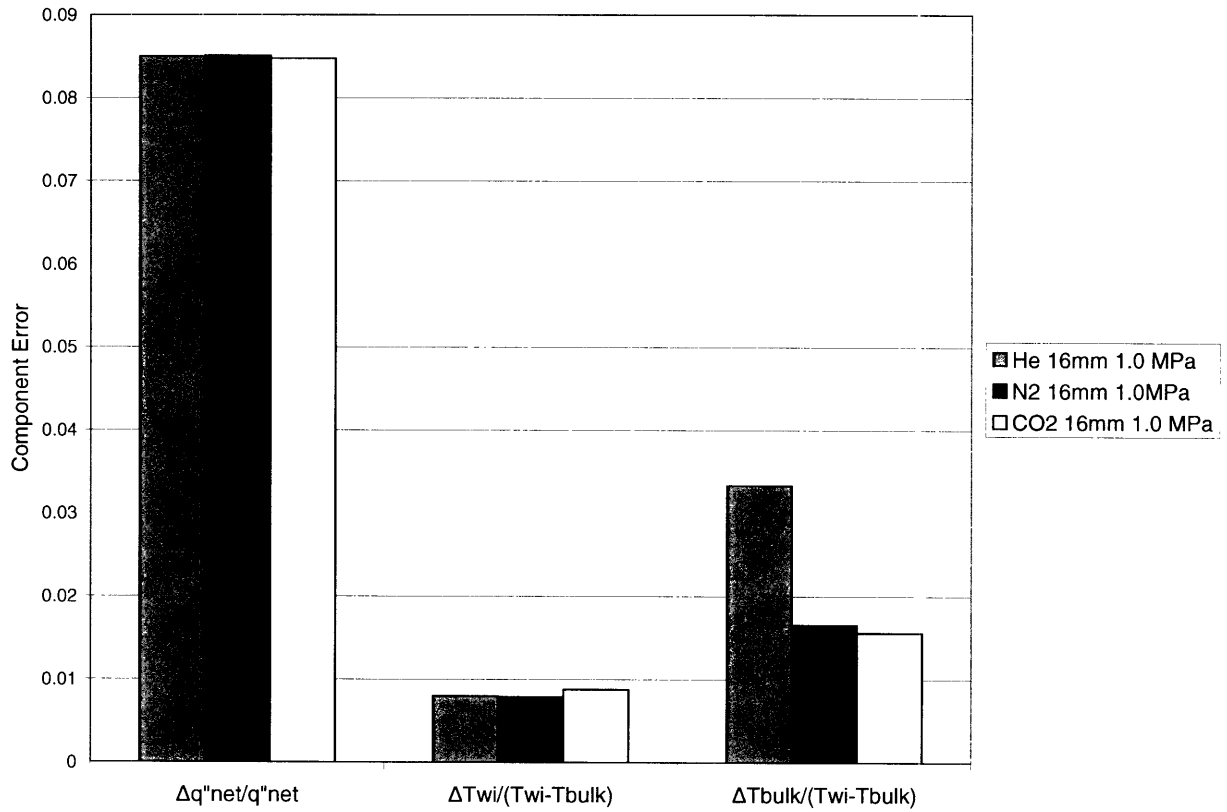
Figure 5-2 Heat transfer coefficient relative uncertainty contributions

5.3.2 Bulk Fluid Temperature

The bulk fluid temperature uncertainty component of the heat transfer coefficient uncertainty has two terms, $(T_{wi} - T_{bulk})$ and ΔT_{bulk}. Having already eliminated $(T_{wi} - T_{bulk})$ as a viable option in reducing the heat transfer coefficient uncertainty we must instead focus on decreasing ΔT_{bulk} in order to reduce the overall uncertainty. ΔT_{bulk} is calculated from the following equation:

$$T_{bulk} = T_i + \frac{(Q_{total} - Q_{loss})}{\dot{m} c_p}$$

(5-31)

$T_i = bulk\ fluid\ temperature\ previous\ node$

The most important aspect of equation 5-31 is the fact that the bulk fluid temperature depends upon the bulk fluid temperature of the previous node. As a result the uncertainty associated with the bulk fluid temperature of the current node incorporates the uncertainty of the bulk fluid temperature of the previous node. This is initially not a problem as the first bulk fluid temperature is measured by a thermocouple and the uncertainty is limited to the intrinsic thermocouple uncertainty of 1°C. However as we progress farther up the test section the uncertainty begins to compound and becomes quite significant. One way to counteract this effect is to calculate the bulk fluid temperatures for the top half of the test section based upon the exit temperature of the fluid as measured by a thermocouple. As a result instead of steadily increasing up the test section the bulk fluid temperature uncertainty increases until the midpoint of the test section and then begins to decrease until the outlet of the test section. The reduced bulk fluid temperature uncertainty is reflected in lower overall values of $\Delta h/h$, which are listed in Table 5.5. It should be noted that reducing the bulk fluid temperature uncertainty has a significant impact upon the helium cases.

Table 5.5 $\Delta h/h$ ranges with reduced bulk fluid temperature uncertainty

Fluid	ID (mm)	Pressure (MPa)	Flow Rate (kg/s)	Deposited Heat (W)	$\Delta h/h$ Range	*$\Delta h/h$ Range
He	16	0.2	2.25E-5	50	0.506-15.29	0.506-5.66
He	16	0.6	1.87E-4	402	0.093-0.232	0.093-0.150
He	16	1.0	4.25E-4	804	0.091-0.130	0.091-0.106
N2	16	0.1	2.54E-4	111	0.112-0.613	0.112-0.600
N2	16	0.2	6.62E-4	251	0.114-0.206	0.114-0.202
N2	16	0.6	1.73E-3	553	0.096-0.126	0.096-0.122
N2	16	1.0	2.69E-3	804	0.093-0.113	0.093-0.108
CO2	16	0.1	4.88E-4	211	0.145-0.251	0.145-0.243
CO2	16	0.2	1.00E-3	327	0.102-0.180	0.102-0.178
CO2	16	0.6	2.60E-3	704	0.094-0.114	0.094-0.109
CO2	16	1.0	4.14E-3	1005	0.092-0.105	0.092-0.101

*denotes reduced bulk fluid temperature uncertainty

5.3.3 Net Heat Flux

There are also two ways of decreasing the net heat flux uncertainty component, either by decreasing $\Delta q_{net}^{''}$ or by increasing $q_{net}^{''}$. The uncertainty term for $\Delta q_{net}^{''}$ is given by the following equation:

$$\Delta q_{net}^{''} = \left[\left(\frac{(q_{total}^{''} - q_{loss}^{''})\Delta d_o}{d_i} \right)^2 + \left(\frac{d_o(q_{total}^{''} - q_{loss}^{''})\Delta d_i}{d_i^2} \right)^2 + \left(\frac{d_o \Delta q_{total}^{''}}{d_i} \right)^2 + \left(\frac{d_o \Delta q_{loss}^{''}}{d_i} \right)^2 \right]^{\frac{1}{2}} \qquad (5\text{-}32)$$

Of the terms in equation 5-32, the only term that is not set by manufacturer or design specifications is the $q_{loss}^{''}$ term. However this term only affects the Δd_o and Δd_i components of the net heat flux uncertainty term, which are negligible when compared to the $\Delta q_{total}^{''}$ and $\Delta q_{loss}^{''}$ components. As a result we must try and increase $q_{net}^{''}$ in order to decrease the overall uncertainty in the heat transfer coefficient. The net heat flux is simply the total heat flux provided by the resistive heating minus the heat flux loss to the environment.

$$q_{net}^{''} = \frac{d_o}{d_i}(q_{total}^{''} - q_{loss}^{''}) \qquad (5\text{-}33)$$

Since our total heat flux is limited by the wall temperature of the test section ($T_{wo} < 650°C$) we will focus on reducing the heat loss to the environment. In our initial design, to reduce heat loss, we wrapped our test section in 10.16 cm thick mineral wool insulation. However, as was discovered in section 4.3, guard heaters for the test section will be necessary to combat the large temperature gradient between the wall of the test section and the ambient air. As mentioned previously, it is not a trivial matter to match the test section wall temperature to the insulation temperature on the inner side of the guard heater (to achieve zero heat flux from the wall) over the entire heated length. As a result in addition to calculating the uncertainty in the heat transfer coefficient assuming no heat loss, we will also do the calculation assuming the guard heaters only reduce the heat loss to ¼ its previous value. The results are listed in Table 5.6. (The uncertainty

reduction in the bulk fluid temperature is incorporated into the reduced heat loss heat transfer coefficient uncertainties)

Table 5.6 Reduced net heat flux uncertainty

Fluid	ID (mm)	Pressure (MPa)	$\Delta h/h$ Range	$*\Delta h/h$ Range	$**\Delta h/h$ Range
He	16	0.2	0.506-5.66	0.513-6.40	0.516-7.46
He	16	0.6	0.093-0.150	0.089-0.152	0.088-0.154
He	16	1.0	0.091-0.106	0.087-0.100	0.085-0.099
N2	16	0.1	0.112-0.600	0.094-0.132	0.089-0.121
N2	16	0.2	0.114-0.202	0.097-0.122	0.090-0.103
N2	16	0.6	0.096-0.122	0.088-0.094	0.086-0.090
N2	16	1.0	0.093-0.108	0.087-0.091	0.086-0.088
CO2	16	0.1	0.145-0.243	0.098-0.111	0.089-0.096
CO2	16	0.2	0.102-0.178	0.092-0.113	0.088-0.097
CO2	16	0.6	0.094-0.109	0.088-0.092	0.086-0.089
CO2	16	1.0	0.092-0.101	0.087-0.090	0.085-0.088

*1/4 of total heat loss **no heat loss

There are a few important aspects of Table 5.6 that should be mentioned. First, reducing the heat loss for the helium calculations has little effect as the major source of uncertainty in the helium heat transfer coefficient calculation is due to the small temperature difference between the bulk fluid temperature and the temperature of the wall. It should also be noted at this point that the trial calculation for helium at 0.2 MPa does not provide heat transfer coefficients with any degree of accuracy; as a result this case will not be incorporated into the experimental trials. Looking at nitrogen and carbon dioxide, we see that the reduction in heat loss has had a significant effect on the uncertainty in the heat transfer coefficient calculations. The most noticeable effects are for the 0.1 and 0.2 MPa cases. For instance in the case of nitrogen at 0.1 MPa, the maximum relative uncertainty, assuming full heat loss, is 0.600, while the maximum uncertainty, assuming no heat

loss, is 0.121. One last important aspect of Table 5.6 is the fact that the differences in relative uncertainty between the two

modified heat losses are negligible. This is important as it allows us some leeway in matching the insulation temperature and wall temperature of the test section through the use of guard heaters.

5.4 Uncertainty Analysis Summary

Accurate determination of heat transfer coefficients for laminar flow is quite challenging, as we are dealing with small amounts of heat deposited in the test section and low mass flow rates. Furthermore since the scope of our experiment involves both laminar and transitional flow regimes in addition to turbulent regimes it is important that we have the same degree of confidence in heat transfer coefficients generated for laminar and transitional flow as we do for turbulent flow. However we expect the laminar and transitional flow regimes to generate less accurate data as the relative uncertainty of the heat transfer coefficient increases with decreasing amounts of heat deposited in the fluid. Figures 5-3 and 5-4 are graphs of the relative uncertainty in the heat transfer coefficient vs. Re and Ra number respectively with reduced uncertainty in bulk fluid temperature and no heat loss. And while it comes as no surprise that laminar flow with low Ra number ranges has the highest relative uncertainty, the uncertainty is of the same magnitude as that calculated for turbulent flows. In fact the difference in the relative uncertainty between laminar and turbulent flows is only a few percentage points, as a result regardless of whether the experimental data is obtained in laminar mixed convection regimes or turbulent forced convection reasonably accurate heat transfer coefficients can be calculated.
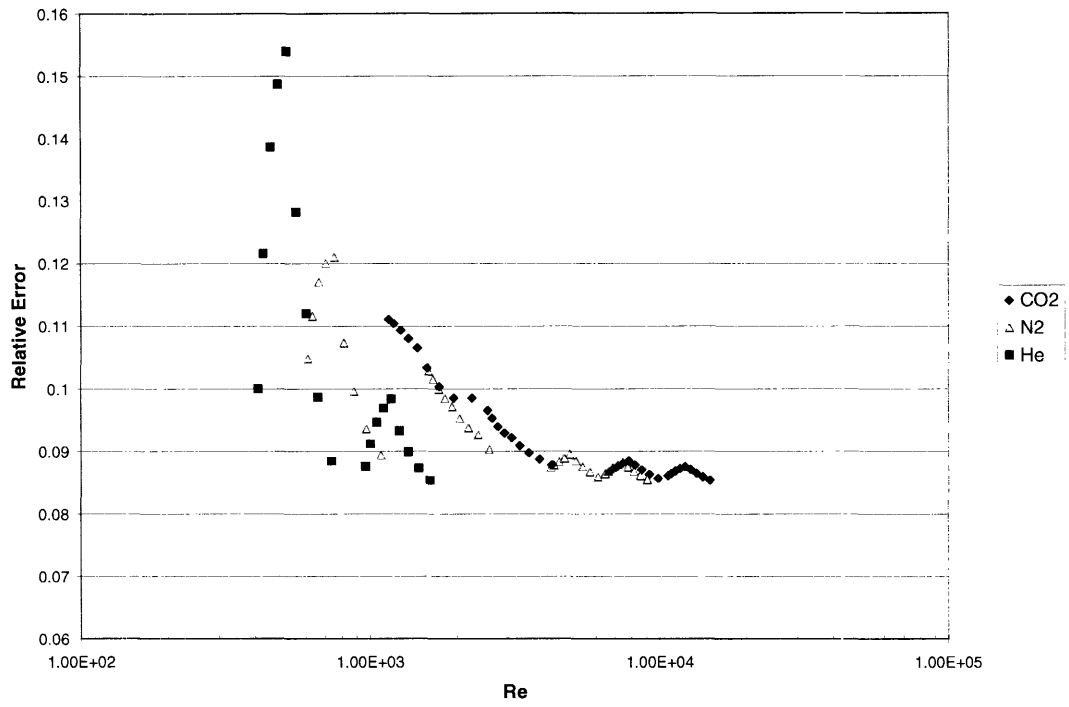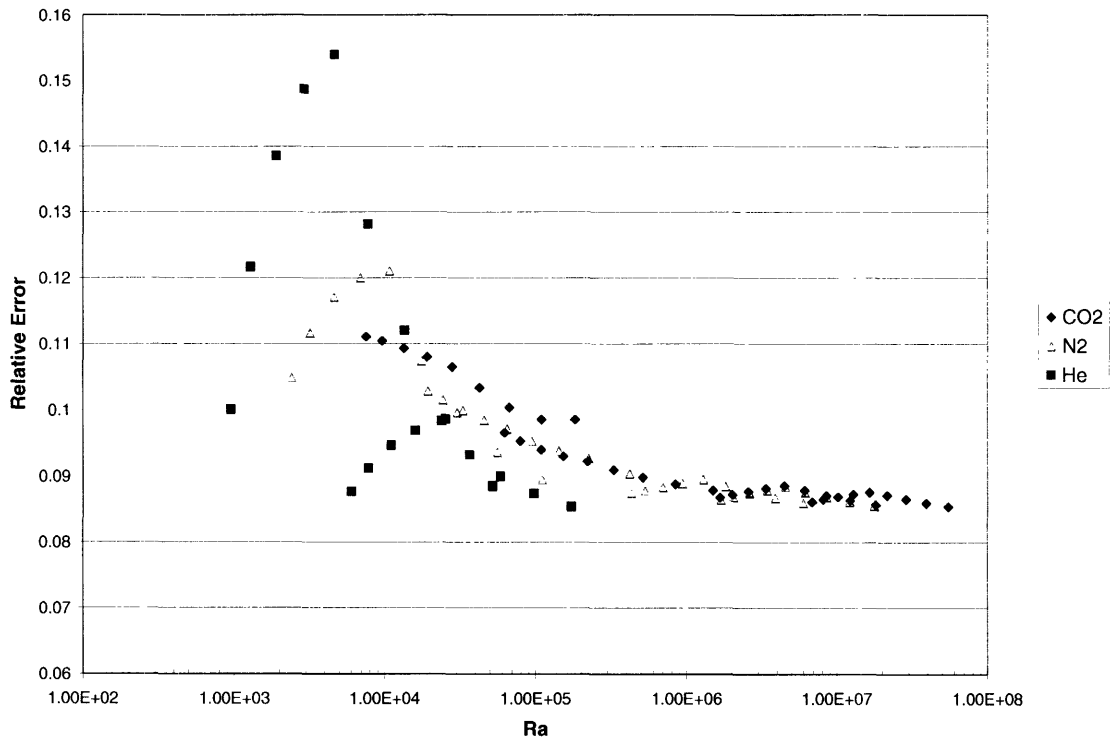
Figure 5-3 Relative uncertainty vs. Re number

Figure 5-4 Relative uncertainty vs. Ra number

75

References

1. Kline, S.J., Mclintock, F.A., "Describing Uncertainties in Single-Sample Experiments", *Mechanical Engineering* Vol. 75 pp. 3-8, 1953

2. NIST Standard Reference Database 12, NIST Thermodynamics and Transport Properties of Pure Fluids - NIST Pure Fluids, Version 5.0, 2000.

6. CONCLUSIONS AND FUTURE WORK

The objective of this thesis seemed simple enough in the beginning, design and build a thermal-hydraulic loop capable of obtaining heat transfer data from the flow regimes mentioned in Table 1-1. However it quickly became apparent that fabrication of such a loop posed some unique problems.

We first encountered problems right out of the gate, as the convection regimes the loop is supposed to operate in are in general not well defined. For instance the boundaries between free, mixed, and forced convection are tentative, they need to be explored experimentally in detail. The hot-wire probe of the test section was included into the design for this very purpose, as obtaining accurate data regarding the fluid temperature and velocity profiles near these boundaries is essential for establishing firm transition regions between flow regimes.

The next problem encountered was due to the fact that the coolant temperature in the GFR prototype loop was above 1000°C for many cases. (See Appendix A for GFR coolant temperatures) However due to calibration of the hot-wire probe for use in the test section the bulk fluid temperature in the model was limited to 450°C. This represented quite a challenge in reproducing the convection flow regimes found in post-LOCA operation of the GFR. We decided to compensate for the lower fluid temperature of the model by varying the test fluid, system pressure, and test section hydraulic diameter. A subsequent scaling analysis of all the possible fluid, pressure, and test section diameter combinations, using LOCA-COLA, verified that the experimental loop can cover all the flow regimes of interest and achieve the ranges of the key non-dimensional parameters encountered in the GFR loop.

Our next stumbling block in the construction of the loop occurred during the design of the instrumentation for the loop. In many of the laminar flow LOCA-COLA simulations the fluid velocity was less than 1 m/s. In these cases the mass flow rate of the fluid was simply too small to be measured by normal flow meters such as an orifice meter, without incurring unacceptable pressure drops. Furthermore accurate measurements of flow velocity are needed initially to calibrate the velocity probe found in the test section. As a result it was decided to measure the fluid velocity by determining the pressure drop in the down-comer section in conjunction with the flow regime. More specifically, a very accurate measurement of the pressure drop will be obtained using a very sensitive differential pressure transducer with a range of 1 Torr. The

velocity probe will be used to identify the flow regime. And finally the flow rate calculated from the previous measurements will be verified by integrating the radial velocity profiles obtained from the probe.

However the most unexpected problem that arose during the design and construction of the loop was the issue of heat loss to the environment. The loop design called for both the test section and hot leg to be insulated, as we were initially concerned that heat loss in the hot leg of the loop would impair our ability to conduct experimental trials under natural circulation conditions. We were not that concerned about heat loss in the test section as the heat lost to the environment could be calculated and the output current from the power supply increased to compensate for the lost heat. However even with the insulation, heat losses to the environment were unacceptable. Natural circulation was impaired as the fluid in the hot leg of the loop still cooled significantly. And for many cases in the test section the heat loss to the environment was comparable to the heat deposited in the fluid. And as was shown in Chapter 5 the experimental data from these cases cannot be used to calculate accurate heat transfer coefficients. As a result we had to implement guard heaters in the insulation to reduce heat losses to acceptable levels.

Finally with the addition of the guard heaters we are left with an experimental loop fully capable of obtaining the necessary data for the formulation of heat transfer correlations in convection flow regimes. That is in fact the next step in the overall project. However the loop is not just limited to collecting data for heat transfer coefficients. The loop may also be used in the future to develop friction factor correlations for transitional flow regimes. Also the addition of the hot-wire probe to the test section has opened up many research possibilities where extensive knowledge of local velocity and temperature fluid profiles is required.

APPENDIX A. GFR CORE DATA

As was stated in the introduction the basis for the experimental loop is a GFR with a block-core configuration. There are numerous core designs for the GFR, however the block-core configuration is currently the preferred choice. However the specifics of the core design are not yet determined. For instance while helium is the preferred choice for coolant, carbon dioxide is also being investigated. And since passive decay heat removal following a LOCA is desired the pressure drop across the core must be minimized. One such core has ceramic hexagonal blocks with coated uranium carbide particles. The hexagonal blocks contain coolant holes with inner diameter of 14.5mm. Tables A-1 and A-2 are descriptions of the relevant core parameters for helium and carbon dioxide coolants, respectively. Furthermore as the core design is not yet definite the coolant channel inner diameter was increased to 16.5mm. Tables A-3 and A-4 are descriptions of the core parameters for helium and carbon dioxide coolants respectively with the larger coolant channel. Finally Tables A-5 (helium) and A-6 (carbon dioxide) were introduced to show reactor data for lower decay power (and thus lower backup pressure) to account for situations where decay heat is reduced to lower levels at longer times into the transient.

Table A-1 Case 1: Helium-cooled CERCER Block Core Reference Design for 600MWth GFR

Geometrical data	
Total number of coolant channels	8662
Coolant channel ID	1.45 cm
Core active height	1.70 m
Bottom reflector + shield height	1m
Top reflector + shield height	1m
Decay heat removal data	
Power rating	600MWth
Decay power for steady state analysis	2% = 12MWth
Coolant	Helium
Core –average outlet temperature limit	850°C
Hot channel outlet temperature limit	1200°C
Peak SiC coating temperature limit	1400°C
Axial peaking factor (chopped cosine)	1.25
Radial peaking factor	1.20
Decay heat mode	natural circulation at backup pressure
Operating decay heat removal loops	2x50%
Height of HEATRIC HX above core	11m
Number of HEATRIC HX channels	2 x 54281
Diameter of HEATRIC HX channel	5mm
Assumed constant wall temperature of HX	107°C
Cross duct connector ID/ length	0.8m/3m
Distance between thermal centers, L_{tc}	13.7m
Key results	
Required Backup Pressure	1.65MPa
Loop flow rate	4.17kg/s
Flow rate through 1 hot channel	3.22E-4 kg/s
Flow rate through 1 average channel	4.81E-4 kg/s
Core pressure drop (includes reflectors)	66.9 Pa
Active core pressure drop	24.2 Pa
Average heat flux	17.889kW/m^2
Core inlet temperature	116 °C
Core average outlet temperature	670.3 °C
Hot channel outlet temperature	1110 °C
Peak cladding temperature	1192°C
Richardson number=g $(\rho_h-\rho_c)$ L_{tc} /$(\rho_c$ $v_{in}^2)$	38.2

Note: Bottom and top reflectors have aligned coolant channels with active core (same ID)

Table A-2 Case 2: CO2-cooled CERCER Block Core Reference Design for 600MWth GFR

Geometrical data	
Same as for helium cooled design (Case 1)	
Decay heat removal data	
Same as for helium cooled design (Case 1)	
Key results	
Required Backup Pressure	1.0MPa
Loop flow rate	20.94kg/s
Flow rate through 1 hot channel	2.31E-3 kg/s
Flow rate through 1 average channel	2.42E-3 kg/s
Core pressure drop (includes reflectors)	237.9 Pa
Active core pressure drop	83.8 Pa
Average heat flux	17.889kW/m^2
Core inlet temperature	368.2 °C
Core average outlet temperature	847.6 °C
Hot channel outlet temperature	962.1 °C
Peak cladding temperature	1149 °C
Richardson number=g $(\rho_h-\rho_c)$ L_{tc} /$(\rho_c$ $v_{in}^2)$	18.4

Table A-3 Case 3: Helium-cooled CERCER Block Core Design with channel ID of 16.5mm

Geometrical data	
Total number of coolant channels	6869*
Coolant channel ID	1.65 cm*
Core active height	2.00 m*
Bottom reflector + shield height	1m
Top reflector + shield height	1m
Decay heat removal data	
Power rating	600MWth
Decay power for steady state analysis	2% = 12MWth
Coolant	Helium
Core –average outlet temperature limit	850°C
Hot channel outlet temperature limit	1200°C
Peak SiC coating temperature limit	1400°C
Axial peaking factor (chopped cosine)	1.25
Radial peaking factor	1.20
Decay heat mode	natural circulation at backup pressure
Operating decay heat removal loops	2x50%
Height of HEATRIC HX above core	11m
Number of HEATRIC HX channels	2 x 54281
Diameter of HEATRIC HX channel	5mm
Assumed constant wall temperature of HX	107°C
Cross duct connector ID/ length	0.8m/3m
Distance between thermal centers, L_{tc}	13.85m*
Key results	
Required Backup Pressure	1.65MPa
Loop flow rate	4.38kg/s
Flow rate through 1 hot channel	4.46E-4 kg/s
Flow rate through 1 average channel	6.38E-4 kg/s
Core pressure drop (includes reflectors)	58.6 Pa
Active core pressure drop	21.9 Pa
Average heat flux	16.851kW/m^2
Core inlet temperature	117.4 °C
Core average outlet temperature	644.9 °C
Hot channel outlet temperature	1023 °C
Peak cladding temperature	1115°C
Richardson number=g $(\rho_h-\rho_c)$ L_{tc} /$(\rho_c$ $v_{in}^2)$	35.8

* Data with asterisk are different from Case 1

Table A-4 Case 4: CO2-cooled CERCER Block Core Design with channel ID of 16.5mm

Geometrical data	
Same as for helium cooled design of Case 3	
Decay heat removal data	
Same as for helium cooled design of Case 3	
Key results	
Required Backup Pressure	1.0MPa
Loop flow rate	21.44kg/s
Flow rate through 1 hot channel	2.99E-3 kg/s
Flow rate through 1 average channel	3.13E-3 kg/s
Core pressure drop (includes reflectors)	223.5 Pa
Active core pressure drop	82.8 Pa
Average heat flux	16.851kW/m^2
Core inlet temperature	371.8 °C
Core average outlet temperature	840.1 °C
Hot channel outlet temperature	951.4 °C
Peak cladding temperature	1115 °C
Richardson number=$g \ (\rho_h - \rho_c) \ L_{tc} \ /(\rho_c \ v_{in}^2)$	18.2

Table A-5 Case 5: Helium-cooled CERCER Block Core Reference design for 600MWth GFR at lower power and pressure

Geometrical data	
Total number of coolant channels	8662
Coolant channel ID	1.45 cm
Core active height	1.70 m
Bottom reflector + shield height	1m
Top reflector + shield height	1m
Decay heat removal data	
Power rating	600MWth
Decay power for steady state analysis	**1% = 6MWth**
Coolant	Helium
Core –average outlet temperature limit	850°C
Hot channel outlet temperature limit	1200°C
Peak SiC coating temperature limit	1400°C
Axial peaking factor (chopped cosine)	1.25
Radial peaking factor	1.20
Decay heat mode	natural circulation at backup pressure
Operating decay heat removal loops	2x50%
Height of HEATRIC HX above core	11m
Number of HEATRIC HX channels	2 x 54281
Diameter of HEATRIC HX channel	5mm
Assumed constant wall temperature of HX	107°C
Cross duct connector ID/ length	0.8m/3m
Distance between thermal centers, L_{tc}	13.7m
Key results	
Required Backup Pressure	**1.03MPa**
Loop flow rate	2.13kg/s
Flow rate through 1 hot channel	1.54E-4 kg/s
Flow rate through 1 average channel	2.46E-4 kg/s
Core pressure drop (includes reflectors)	76.4 Pa
Active core pressure drop	18.6 Pa
Average heat flux	8.9447kW/m^2
Core inlet temperature	107 °C
Core average outlet temperature	650.2 °C
Hot channel outlet temperature	1144 °C
Peak cladding temperature	1180°C
Richardson number=g $(\rho_h-\rho_c)$ L_{tc} $/(\rho_c$ $v_{in}^2)$	60.2

Note: Bottom and top reflectors have aligned coolant channels with active core (same ID)

Table A-6 Case 6: CO2-cooled CERCER Block Core Reference Design for 600MWth GFR at lower power and pressure

Geometrical data	
Total number of coolant channels	8662
Coolant channel ID	1.45 cm
Core active height	1.70 m
Bottom reflector + shield height	1m
Top reflector + shield height	1m
Decay heat removal data	
Power rating	600MWth
Decay power for steady state analysis	**1% = 6MWth**
Coolant	CO2
Core –average outlet temperature limit	850°C
Hot channel outlet temperature limit	1200°C
Peak SiC coating temperature limit	1400°C
Axial peaking factor (chopped cosine)	1.25
Radial peaking factor	1.20
Decay heat mode	natural circulation at backup pressure
Operating decay heat removal loops	2x50%
Height of HEATRIC HX above core	11m
Number of HEATRIC HX channels	2 x 54281
Diameter of HEATRIC HX channel	5mm
Assumed constant wall temperature of HX	107°C
Cross duct connector ID/ length	0.8m/3m
Distance between thermal centers, L_{tc}	13.7m
Key results	
Required Backup Pressure	**0.4MPa**
Loop flow rate	10.47kg/s
Flow rate through 1 hot channel	1.20E-3 kg/s
Flow rate through 1 average channel	1.21E-3 kg/s
Core pressure drop (includes reflectors)	227.3 Pa
Active core pressure drop	46.7 Pa
Average heat flux	8.9447kW/m^2
Core inlet temperature	226 °C
Core average outlet temperature	727 °C
Hot channel outlet temperature	823 °C
Peak cladding temperature	1147°C
Richardson number=g $(\rho_h-\rho_c)$ L_{tc} $/(\rho_c$ $v_{in}^2)$	22.8

Note: Bottom and top reflectors have aligned coolant channels with active core (same ID